Title:

CD226^{+} macrophages arise from MDP-derived monocytes and regulate lipid metabolism.

Authors:

Alexandre Gallerand[1]*, Zakariya Caillot[1], Frederike Westermann[2], Selma Tuzlak[2], Sacha Grenet[1], Marina Terekhova[3], Alexia Castiglione[1], Thomas Pilot[4], Laurent L'homme[5], Kerim Acil[6], Lorlana Leporati[1], Margaux Giacchero[1], Eloïse Goës[1], Maxime Franceschini[1], Sebastien Fleury[5], Evy Boré[1], Michael Chang[7], Bastien Dolfi[1], Fairouz N. Zair[1], Audrey Bennetot[1], Zandile Mlamla[8], David Voehringer[9], Matthias Mack[10], Jaap G. Neels[1], Joel Haas[5], David Dombrowicz[5], Jesse W. Williams[7], David Masson[4], Elvira Mass[6], Maxim N. Artyomov[3], Burkhard Becher[2], Adeline Bertola[1], Stoyan Ivanov[1]*

*equal contribution.

Affiliations :

1 Université Côte d'Azur, CNRS, Adipo-Cible Research Study Group, LP2M, Nice, France.
2 Experimental Immunology, University of Zurich, Switzerland.
3 Department of Pathology and Immunology, Washington University in St. Louis, School of Medicine, St. Louis, MO, USA.
4 Université Bourgogne Franche-Comté, LNC UMR1231, F-21000 Dijon, France.
5 Univ. Lille, INSERM, CHU Lille, Institut Pasteur de Lille, U1011-EGID, 59000 Lille, France.
6 Developmental Biology of the Immune System, Life and Medical Sciences (LIMES) Institute, University of Bonn, Bonn, Germany.
7 Center for Immunology, Department of Integrative Biology and Physiology, University of Minnesota Medical School, Minneapolis, MN, USA.
8 Faculté de Médecine de Dijon, Diviomics (Plateforme de Lipidomique-uBourgogne), UMS Biosand, INSERM UMR1231, LabEx LipSTIC, UFR des Sciences de Santé de Dijon, France.
9 Department of Infection Biology, University Hospital Erlangen and Profile Center Immunomedicine (i-MED) of the Friedrich-Alexander University Erlangen-Nuremberg (FAU), Erlangen, 91054, Germany.
10 Department of Nephrology, Regensburg University Medical Center, Regensburg 93042, Germany.

Correspondence to:

Stoyan.ivanov@univ-cotedazur.fr
Alexandre.gallerand@univ-cotedazur.fr

Abstract

Macrophages are innate immune cells present in all tissues, in which they participate in immune responses and maintenance of tissue homeostasis. They develop either from embryonic precursors or from circulating monocytes, and their origin impacts their functions. We previously observed robust recruitment of monocytes to brown adipose tissue in which they could differentiation into two distinct macrophage subsets identifiable by CD206 or CD226 expression. In the present study, we investigated monocyte differentiation pathways in brown adipose tissue and the function of monocyte-derived macrophages. Fate mapping analysis revealed a low contribution of GMP- and a high contribution of MDP-derived

monocytes to the CD226^{high} macrophage subset. Importantly, adoptive transfer experiments demonstrate that MDP- but not GMP-derived monocytes are pre-conditioned to give rise to CD226^{high} macrophages. We found that MDP-derived CD226^{high} macrophages were also present in other tissues including peritoneal cavity, adrenal glands and all adipose depots. CD226^{high} macrophages were regulated by both GM-CSF and CSF1R. Genetic depletion of CD226^{high} macrophages caused increased BAT and plasma triglyceride content. We thus identify CD226^{high} MDP-derived macrophages as a new myeloid cell type conserved across tissues and tied to lipid metabolism homeostasis.

Introduction

Macrophages are innate immune cells observed in all organs [1]. These cells originate from embryonic or bone marrow precursors [1,2]. In adulthood, the proportion of monocyte- and embryonically-derived macrophages varies in different tissues. For example, brain macrophages are exclusively derived from embryonic precursors and their pool is sustained through proliferation, while in gut, lung and spleen, macrophages are more frequently renewed by recruitment of blood monocytes [2,3]. While brown adipose tissue macrophages are initially seeded during embryogenesis [4], they are diluted through monocyte recruitment after birth [4,5].

Brown adipose tissue (BAT) is actively involved in heat generation by adaptive thermogenesis [6]. UCP1 (Uncoupling Protein 1) expression and high mitochondria content are BAT hallmarks [7]. Previous work established that BAT contains several macrophage subsets that heavily rely on CCR2-dependent monocyte recruitment for their maintenance [5]. Nevertheless, the functions of BAT macrophage subsets remain ill-characterized. A subset of $CX3CR1^{+}$ BAT macrophages regulates neuron network density and subsequently the thermogenic response [8]. Adipose tissue macrophage depletion with a CSF1R-blocking antibody was associated with a decreased local lipid content [9]. Yet, whether this function is fulfilled by a selective macrophage subset, or requires the coordinated contribution of several macrophage populations, is not yet established.

Monocytes are generated in the bone marrow through a tight spatially and temporally regulated multistep process named myelopoiesis. Two major monocyte subsets are present in mice and express distinct phenotypic markers [10,11]. $Ly6C^{high}$ classical monocytes are recruited to peripheral tissues at steady state and upon inflammation and contribute to the maintenance of tissue resident macrophages [3]. $Ly6C^{low}$ non-classical monocytes contribute to blood vessel health by secreting growth factors and play a pivotal role during cancer metastasis [12-14]. The majority of blood monocytes originate from granulocyte-monocyte precursors (GMPs) [3]. However, an alternative pathway generating monocytes and dependent on monocyte-dendritic cell precursors (MDPs) has been also proposed [15,16]. We previously established that BAT macrophages are constantly supplied by blood monocytes, yet whether GMP- and MDP-derived monocytes give rise preferentially or exclusively to selective BAT macrophage subsets is yet not established.

In the present study, we report that $CD226^{high}$ macrophages are a unique macrophage subset that is conserved across tissues, including adipose tissues and serosal cavities. These cells particularly accumulate in thermogenic adipose depots in which they regulate triglyceride homeostasis. $CD226^{high}$ macrophages arise in majority from MDP-derived monocytes. Invalidating *Csf1r* or *Csf2* leads to a partial reduction of $CD226^{high}$ macrophage numbers in adipose tissue and peritoneal cavity, suggesting that this atypical macrophage population relies on both CSF1 and CSF2 for their generation and maintenance. Together, these results indicate that the $CD226^{high}$ macrophages are a unique myeloid cell population controlling lipid metabolism both locally and systemically.

Results

$CD226^{high}$ macrophages arise from monocytes but show low contribution from GMPs.

We recently demonstrated that BAT contained numerous immune cells by using single-cell RNA sequencing (scRNA-seq) analysis [5]. BAT contained several monocyte, macrophage

104 and dendritic cell (DC) clusters (**Figure S1a**). Among those cells, *Itgam* (CD11b) mRNA was
105 expressed by the majority of the clusters (**Figure S1b**). We identified three monocyte subsets
106 (clusters 2, 3 and 4) in BAT characterized by their relative expression of *Ly6c2* and *Nr4a1*
107 mRNA (**Figure S1b**). Cluster 2 contained Ly6C^{low} monocytes and cluster 4 included Ly6C^{high}
108 monocytes. Furthermore, we predicted that BAT contained 4 well-defined macrophage
109 subsets (clusters 5, 6, 7 and 8). Cluster 5 macrophages expressed *Cd226* mRNA and several
110 genes encoding for proteins involved in extracellular matrix remodeling and these cells were
111 initially named "Matrix" macrophages (**Figure S1c**) [5]. Cluster 6 was the larger macrophage
112 cluster (**Figure S1c**). Cluster 6 macrophages highly expressed genes previously associated with
113 macrophage alternative polarization in response to IL-4 (*Mrc1*, *Lyve1*, *CD163*) (**Figure S1c**).
114 These cells were called CD206^{high} macrophages (**Figure S1c**) [5]. Two additional macrophage
115 clusters were also identified (clusters 7 and 8) and were characterized by the expression of
116 enzymes involved in lipid metabolism (*Lpl* and *Plin2*). To validate at the protein level the
117 predicted myeloid cell diversity in BAT, we developed a gating strategy and used spectral flow
118 cytometry. Macrophages were identified as CD45$^+$ F4/80$^+$ MerTK$^+$ cells (**Figure S1d**).
119 According to our scRNA-seq data predictions, matrix macrophages were found to highly
120 express CD226 and had low CD64 (Fcgr1) expression (**Figures 1a, S1c-d**). CD206^{high}
121 macrophages were found to highly express both CD206 and CD64 (**Figures S1c-e**). A fraction
122 of these cells also co-expressed Lyve1 and Timd4, suggesting long tissue residency (**Figures**
123 **S1c-e**). Uptake of intravenously injected TRITC-Dextran indicated that CD206^{high} macrophages
124 displayed phagocytic behavior and were likely associated with blood vessels while CD226^{high}
125 macrophages showed lower dextran uptake (**Figure S1f**). Since we could not define distinct
126 membrane markers for macrophage clusters 7 and 8, these cells were identified as CD45$^+$
127 F4/80$^+$ MerTK$^+$ CD206$^-$ CD226$^-$ cells (DN macrophages). Ly6C^{high} monocytes were defined as
128 CD45$^+$ MerTK$^-$ Ly6C$^+$ CD11b$^+$ Ly6G$^-$ cells (**Figure S1d**). We also found cells corresponding to
129 conventional DC (cDC) subsets. cDC2 were identified as CD45$^+$ MerTK$^-$ CD11c$^+$ MHC-II$^+$ CD11b$^+$
130 cells while cDC1 were CD45$^+$ MerTK$^-$ CD11c$^+$ MHC-II$^+$ CD24$^+$ (**Figure S1d**).
131 Next, we aimed at defining the developmental connections between macrophage
132 subsets. We previously demonstrated a high contribution of blood monocytes to the BAT
133 macrophage pool [5]. Using Slingshot analysis of BAT monocyte and macrophage clusters, we
134 predicted that monocytes could generate two terminally differentiated BAT populations:
135 CD226^{high} and CD206^{high} macrophages (**Figure 1a**). Macrophage clusters 7 and 8 appeared as
136 intermediate stages of differentiation towards the generation of clusters 5 and 6 (**Figure 1a**).
137 Importantly, Timd4 expression was high selectively in CD206^{high} macrophages, suggesting that
138 these cells could be, at least partially, from an embryonic origin (**Figure 1b**). Timd4 expression
139 was low on DN and CD226^{high} macrophages further supporting their monocyte origin (**Figure**
140 **1b**). Our scRNA-seq data revealed that *Cx3cr1* mRNA was highly expressed in BAT monocytes
141 but not macrophages (**Figure S1c**). To assess CX3CR1 protein expression on BAT myeloid cells,
142 we used CX3CR1$^{GFP/+}$ mice [17]. BAT monocytes and DN macrophages highly expressed CX3CR1
143 (**Figure 1c**). A fraction of CD206^{high} macrophages (nearly 25%) was also GFP$^+$ (**Figure 1c**). GFP
144 expression level was the lowest in BAT CD226^{high} macrophages (**Figure 1c**). These
145 observations suggested that monocytes could differentially contribute to BAT macrophage
146 subsets, with a lower contribution to the CD206^{high} macrophage subset.
147 We next used genetic pulse-chase experiments to investigate monocyte contribution to
148 BAT macrophage populations. For this purpose, *CCR2^{CreERT2}; R26$^{LSL-tdT}$; CX3CR1$^{GFP/+}$* mice were
149 administered with tamoxifen (TAM) and analyzed 48 hours later (**Figure 1d**). We analyzed the
150 appearance of tdTomato$^+$ cells in macrophage subsets and found that around 60% of

151 CX3CR1^{GFP+} cells were labelled at this time point (**Figure 1d**). Importantly, the majority of
152 CX3CR1-expressing CD206^{high} BAT macrophages were not tdTomato^{+}, suggesting that this
153 population is not monocyte-derived, or its replenishment rate is slower in comparison to
154 CD206^{-} macrophages (**Figure 1d**). Among CX3CR1^{-} BAT macrophages, tdTomato labelling was
155 lower, as only around 12% were marked, and these cells were CD206^{-} (**Figure 1d**).
156 To test any potential link between BAT CX3CR1^{+} and CX3CR1^{-} myeloid cells, we
157 administered TAM in *CX3CR1$^{CreERT2/GFP}$; R26$^{LSL-tdT}$* mice and followed tdTomato expression in
158 BAT macrophages (**Figure 1e**). 2 days post-TAM administration, 66.6% of tdTomato^{+} BAT
159 macrophages were CX3CR1^{GFP+} (**Figure 1e**). This percentage dropped to 33.8% 7 days after
160 TAM (**Figure 1e**). We could thus demonstrate that monocytes are continuously recruited to
161 BAT in which they first give rise to CX3CR1^{+} CD206^{-} CD226^{-} macrophages, that then
162 differentiate to CX3CR1^{-} macrophages, corresponding to CD206^{high} and CD226^{high} cells.
163 The majority of blood monocytes arise from GMPs [3]. To track GMP-dependent
164 monocyte differentiation into BAT macrophages, we used *Ms4a3^{CreERT2}; R26$^{LSL-tdT}$* mice [3]. Mice
165 were gavaged with TAM and the frequency of tdTomato^{+} cells in each macrophage subset
166 was defined in a time-course manner. As previously described [3], we observed that blood
167 monocyte labelling efficiency reached 90-95% (data not shown). 3 days after the last TAM
168 administration, around 70% of BAT monocytes were tdTomato^{+} (**Figure 1f**). This percentage
169 rapidly decreased and reached 0% at day 17 due to the recruitment of unlabeled bone
170 marrow-derived monocytes (**Figure 1f**). The labelling of DN BAT macrophages peaked at day
171 3, when 20% of cells were labelled, further supporting that this population depended on
172 blood monocyte recruitment to sustain (**Figure 1f**). Of interest, the labelling of BAT CD226^{high}
173 macrophages peaked at day 10 when labeling of DN macrophages was already decreasing
174 (**Figure 1f**). This demonstrated that while CD226^{high} macrophages rely at least partially on
175 GMP-derived monocytes for their maintenance, their differentiation trajectory occurs over a
176 longer time frame. We detected very low contribution (less than 3%) of GMP-derived blood
177 monocytes to BAT CD206^{high} macrophages (**Figure 1f**). However, it remains elusive whether
178 early postnatal bone marrow-derived monocytes contribute to a long-lived pool of BAT-
179 resident macrophages.
180 We next analyzed the presence of CD206^{high} and CD226^{high} at postnatal days (p)0, p7,
181 p14, p21, and p28 in C57BL/6J mice. CD206^{high} macrophages were the only subset present at
182 birth (p0), and CD226^{high} and DN macrophages only started to accumulate in BAT between
183 p14 and p21 (**Figure S2a**). DN macrophages slowly accumulated over time, diluting CD206^{high}
184 macrophages, while proportions of CD226^{high} macrophages remained constant (**Figure S2b**).
185 To address the ontogeny and longevity of BAT macrophages at these pre- and postweaning
186 stages, we utilized the "*double fate-mapper*" mouse model that enables the simultaneous
187 labelling of macrophages derived from the yolk sac pre-macrophages (pMacs) and GMPs[18] .
188 In this *double fate-mapper*, yolk sac-derived, tissue-resident macrophages express YFP via the
189 *Tnfrsf11a^{Cre}; Rosa26$^{LSL-YFP}$* lineage tracer [19], while GMP-derived macrophages are labelled with
190 tdTomato using the *Ms4a3^{Flp}; Rosa26$^{FSF-tdT}$* model (**Figure 1g**). The *double-fate mapper* also
191 enables the distinction between short-lived (tdTomato^{+}) and long-lived GMP-derived
192 macrophages (YFP^{+} tdTomato^{+}): as *Tnfrsf11a* is a macrophage core gene, its upregulation and
193 concomitant expression of the Cre recombinase leads to YFP labelling of macrophages that
194 take up tissue residency. YFP^{+} tdTomato^{+} CD206^{high} only started appearing at p14 at low
195 frequencies (**Figure 1h**). At p21, we observed a transient influx of single tdTomato^{+}
196 macrophages (~8%), and a concurrent increase of YFP^{+} tdTomato^{+} CD206^{high} macrophages to
197 18%, indicating that weaning and/or food uptake leads to a recruitment of GMP-derived

198 macrophages that become tissue-resident (**Figures 1g and S2c**). Albeit only very few CD226^{high}
199 macrophages were detected at birth, all were single YFP^{+} (**Figures 1h and S2c**), suggesting
200 that they develop from pMacs that were still circulating at birth and seeded the tissue in the
201 first week of life. However, we observed a transient input of YFP^{+} tdTomato^{+} CD226^{high}
202 macrophages (18%), similar to CD206^{high} macrophages. However, at p21, the GMP-derived,
203 long-lived cells disappeared, and we detected an unlabeled CD226^{high} macrophage population
204 (~30%), indicating a GMP-independent influx of short-lived macrophages. Analysis of 8-week-
205 old Ms4a3^{Flp} reporter mice showed that GMP contribution to BAT monocytes reached only
206 ~80%, compared to ~95% in blood [3] (**Figures 1i-j**). This observation suggests that GMP-
207 independent monocytes could be recruited to BAT. While 70% of DN macrophages were
208 labeled, only 30% and 40% of CD226^{high} and CD206^{high} macrophages, respectively, were
209 labeled (**Figure 1j**). In summary, these data demonstrate that all BAT-resident macrophages
210 are embryonically-seeded, with the establishment of macrophage subset heterogeneity in the
211 first weeks of life.
212 Lastly, we sought to define whether recruitment of monocytes is essential to the
213 maintenance of BAT macrophage subsets. To answer this question, we treated mice with anti-
214 CCR2 MC-21 antibody allowing to efficiently deplete classical monocytes [20]. In BAT, we
215 observed an almost complete monocyte depletion 24 hours after MC-21 treatment, in
216 comparison to control animals (**Figure S2d**). Continuous MC-21 administration kept
217 monocytes absent from BAT over time (**Figure 1k**). DN macrophage numbers tended to
218 decrease at day 1 post MC-21 injection, while CD206^{high} and CD226^{high} macrophage
219 abundance only started decreasing at day 2 post MC-21 administration (**Figure 1k**).
220 Monocytes and all macrophage populations were decreased after 5 days of MC-21 treatment
221 (**Figure 1k**). These data indicated that BAT macrophages strongly depend on monocyte flux
222 to sustain constant numbers, albeit depletion of CD226^{high} and CD206^{high} macrophages was
223 slower than DN cells (**Figure 1k**). Overall, our findings demonstrate the existence of robust
224 monocyte contribution to BAT CD226^{high} macrophages through a minor GMP-dependent and
225 a major GMP-independent cellular pathway.
226
227 **CD226^{high} macrophages preferentially arise from MDP-derived monocytes.**
228 A recent report suggested that a proportion of blood monocytes arise from a GMP-
229 independent and MDP-dependent precursor [15]. However, these observations relied on
230 scRNA-seq data and adoptive transfer experiments, and genetic tools allowing to track MDPs
231 and their progeny are lacking. We thus used RNA sequencing data from the Immgen
232 consortium to compare GMPs to MDPs and identify subset-specific genes that could be
233 targeted using existing genetic tools (**Figure S3a**). *Flt3* and *Ccr2* were present among the 30
234 most differentially expressed genes, however blood monocytes can be highly labeled using
235 Flt3^{Cre} and Ccr2^{Cre} mice due to expression of these genes upstream and downstream of
236 monocyte progenitors, making them incompatible with progenitor-restricted fate mapping.
237 However, we identified *Clec9a* as a gene with higher expression in MDPs compared to GMPs
238 (**Figure S3a**). Indeed, *Clec9a* appeared to be expressed in MDPs and CDPs but not in upstream
239 progenitors nor GMPs and monocytes (**Figure 2a**). We thus crossed Clec9a^{iCre} mice [21] to R26^{TdT}
240 mice and analyzed bone marrow progenitor labelling efficiency (**Figure S3b**). Our data
241 revealed that 40% of CDPs and 10% of MDPs were tdTomato^{+} (**Figure 2b**). cMoPs were not
242 labelled and remained tdTomato^{-} (**Figure 2b**). We also detected a population of bone marrow
243 monocytes (around 5%) that expressed tdTomato (**Figure 2b**). These data indicated that
244 Clec9a labelling in monocytes could reflect a MDP-dependent origin.

We next analyzed the presence of tdTomato$^+$ cells in peripheral blood immune cell populations in Clec9a^{iCre} R26^{tdT} mice (**Figure S3c**), demonstrating that approximately 5% of blood monocytes were labelled (**Figure 2d**), mirroring blood monocyte labeling using Ms4a3^{Flp} mice. Equal tdTomato labeling was observed in Ly6C^{high} and Ly6C^{low} blood monocytes (**Figure 2d**). However, no additional blood immune cells were labelled. Indeed, neutrophils, B cells, T cells (both CD4$^+$ and CD8$^+$ subsets) and Natural Killer (NK) cells remained tdTomato$^-$ (**Figure S3d**). To verify whether tdTomato$^+$ blood CD11b$^+$ CD115$^+$ Ly6C^{high} cells were indeed monocytes rather than pre-DCs, we crossed Clec9a^{iCre} R26^{TdT} mice with Zbtb46^{GFP} reporter mice. We confirmed that tdTomato expression was present in bone marrow CD11b$^-$ CD34$^+$ CD16/32$^-$ Flt3$^+$ cKit$^+$ Zbtb46^{GFP-} progenitors, containing MDPs (**Figure S3e**). CD11b$^-$ CD34$^+$ CD16/32$^-$ Flt3$^+$ cKit$^-$ Zbtb46^{GFP+} progenitors, containing CDPs, also highly expressed tdTomato (**Figure S3e**). In blood, both tdTomato$^+$ and tdTomato$^-$ Ly6C^{high} monocytes lacked GFP signal (**Figure 2d**). We then analyzed the spleen since this tissue contains DCs that could act as internal positive control for GFP expression (**Figure 2e**). Ly6C^{high} monocytes constituted around 6% of tdTomato$^+$ cells in this organ, and again these cells lacked expression of Zbtb46^{GFP} (**Figure 2e**). We next sought to analyze Clec9a^{iCre} labeling among tissue macrophages and observed that the majority (70-80%) of BAT CD226^{high} macrophages were labelled with tdTomato (**Figure 2f**). These data mirrored the labelling percentage documented in Ms4a3^{Flp}; R26^{tdTomato} mice, suggesting that MDP-derived monocytes rather than GMP-derived monocytes could be the main progenitors of CD226^{high} macrophages.

We next asked whether a similar labeling pattern could be observed in macrophages from other tissues. Small peritoneal cavity macrophages (SCMs) were demonstrated to express CD226 and to heavily rely on monocytes for their maintenance [22]. These cells reside in the peritoneal cavity where they share the local microenvironment with large peritoneal cavity macrophages (LCMs), yet LCMs and SCMs display specific transcriptional signatures (Immgen.org) (**Figure 2g**). We compared the transcriptomic profile of BAT CD226^{high} macrophages to that of peritoneal LCMs and SCMs and found that they strongly resembled SCMs (**Figure 2g**), indicating that the CD226^{high} macrophage subset could be conserved across several tissues. Peritoneal wash (PW) SCMs and BAT CD226^{high} macrophages showed a similar labeling pattern in Ms4a3^{Flp}; R26^{tdTomato} mice with only around 25% of these cells being labeled (**Figure 2h**). Curiously, around 20% of monocytes were labeled in PW from Clec9a^{iCre}; R26^{tdTomato} mice (**Figure 2i**) compared to 5% in blood. While only a small fraction of LCMs was tdTomato$^+$, around 75% of SCMs expressed the tdTomato reporter (**Figure 2i**). We confirmed that this was not due to *Clec9a* mRNA expression in SCMs (**Figure S3f**) nor BAT CD226^{high} macrophages (**Figure S3g**). Taken together, these data suggested that MDP-derived monocytes give preferentially rise to peritoneal cavity and BAT CD226^{high} macrophages.

Based on the observation that MDP-derived monocytes had a higher contribution to CD226^{high} macrophages than GMP-derived monocytes across tissues, we hypothesized that monocyte differentiation trajectories were pre-conditioned by their origin. To test this hypothesis, we cell-sorted total splenic monocytes from Clec9a^{iCre} R26^{TdT} mice (CD45.2$^+$ cells) and transferred them intraperitoneally into CD45.1 host mice without prior treatment (**Figure 2j**). 7 days after injection, the presence and phenotype of donor CD45.2 cells were analyzed by flow cytometry. We observed that tdTomato$^-$ donor cells preferentially gave rise to LCMs (**Figures 2j and 2k**). In striking contrast, tdTomato$^+$ cells generated both CD226^{high} SCMs and LCMs (**Figures 2j and 2k**). Even though only ~7% of donor cells were tdTomato$^+$ (**Figure 2j**), 60% of donor CD226^{high} SCMs were tdTomato$^+$ (**Figure 2k**). These results demonstrate that monocyte origin influences their ability to generate specific macrophage subsets in tissues.

292 Finally, we sought to confirm that Clec9a^{iCre} and Ms4a3^{Flp} mice allowed to label two
293 different lineages. For this purpose, we crossed Ms4a3^{Flp}; R26$^{FSF\text{-}tdTomato}$ mice Clec9a^{iCre} R26$^{LSL\text{-}YFP}$ mice to generate a double reporter system in which MDP-derived macrophages would be
295 YFP-labeled and GMP-derived macrophages would be tdTomato-labeled (**Figure 2l**). We
296 observed non-overlapping expression of YFP and tdTomato among BAT CD226^{high}
297 macrophages (**Figure 2l**). Even though overall YFP labeling was lesser than what we measured
298 using Ai14 reporter mice (**Figure S3h**) as expected, most YFP^{+} cells were CD226^{high} and most
299 tdTomato^{+} cells were CD206^{high} or CD206^{-}CD226^{-} macrophages in BAT (**Figure 2l**). Both YFP
300 and tdTomato labeling were very low or absent in resident macrophage populations such as
301 alveolar macrophages, Kupffer cells and microglia (**Figure S3i**). Overall, our data validate
302 Clec9a^{iCre} mice as suitable tools for fate mapping MDP-derived monocytes and macrophages
303 and demonstrate that CD226^{high} macrophages are a population with mixed monocytic origin
304 dominated by the MDP lineage.
305
306 **CD226^{high} macrophages are conserved across tissues and enriched in thermogenic adipose**
307 **depots.**
308 We observed that a myeloid cluster also expressed CD226 in our previously published
309 single cell RNA-sequencing dataset of adrenal gland (AG) immune cells [23]. A recent direct
310 comparison between murine and human peritoneal cavity immune cells revealed that
311 CD226^{high} SCMs are conserved in humans and show similarities with human type 2 dendritic
312 cells [24]. Based on these observations, we aimed to decipher (i) whether CD226^{high}
313 macrophages were present in other tissues beyond BAT and peritoneal cavity and (ii) whether
314 these cells might share part of their signature with dendritic cells. To answer these questions,
315 we integrated mononuclear phagocytes from previously published scRNA-seq datasets from
316 BAT [5], AG [23] and peritoneal cavity [24], as well as splenic Flt3^{+} cells containing plasmacytoid and
317 conventional (type 1, 2 and 3) dendritic cells [25] (**Figure 3a**). CD226^{+} macrophages were
318 identified in BAT, AG and peritoneal cavity and they clustered together (**Figures 3a-b**).
319 Importantly, CD226^{high} cells clustered away from recently-described type 3 dendritic cells
320 (cDC3) that express markers common with the macrophage lineage including CD16/32 and
321 CD115 [25] (**Figure 3b**). Indeed, CD226^{high} macrophages lacked expression of the core signature
322 of cDC3 (**Figure 3c**). We next explored a publicly available dataset generated by the Tabula
323 Muris consortium [26] to test whether CD226^{+} macrophages could be found in additional
324 tissues. We generated a gene set named "CD226^{high} signature", comprising the 50 genes with
325 highest differential expression between BAT CD226^{high} macrophages and other BAT immune
326 cells. This signature was absent in most of the dataset, except for one group of cells (**Figure**
327 **S4a, left**). Indeed, cells highly expressing this gene set clustered together (**Figure S4a, right**).
328 These cells were predicted to be myeloid cells and in particular macrophages (**Figure S4b**).
329 They were enriched in adipose tissue and limb muscle, even though they were also detected
330 at a lower degree in heart, trachea and mammary glands (**Figure S4b**). In agreement with our
331 data presented in Figure S2a, the abundance of CD226^{high} macrophages did not depend on
332 biological sex nor age (**Figure S4b**).
333 Next, we generated a genetic model to target and track CD226^{+} macrophages across
334 tissues. Resistin like alpha (*Retnla*) appeared to be a hallmark gene for both BAT and
335 peritoneal CD226^{+} macrophages [5,22]. We could confirm that *Retnla* was highly expressed in
336 CD226^{high} macrophages in our integrated dataset (**Figure 3d**). Thus, we crossed Retnla^{Cre} mice
337 [27] with *R26$^{LSL\text{-}tdTomato}$* reporter animals. In these mice, tdTomato expression was exclusively
338 detected in CD45^{+} cells in BAT (**Figure 3e**). Among CD45^{+} cells, tdTomato expression was

339 highly enriched in myeloid F4/80^{+} cells (**Figure 3e**). Among BAT macrophages, the highest
340 tdTomato expression was detected in CD226^{high} macrophages, although lower labelling was
341 also detected in BAT CD206^{high} and DN macrophages (**Figure 3e**). Blood monocytes were not
342 labeled with tdTomato (**Figure 3e**). We could confirm that only cells resembling macrophages
343 expressed tdTomato in BAT by confocal microscopy, and that adipocytes were not labelled
344 (**Figure 3f**). In the peritoneal cavity, we found that tdTomato was expressed by SCMs but not
345 by dendritic cells (**Figure S4c**). We next investigated the presence of CD226^{high} macrophages
346 in different adipose tissue depots and compared brown (BAT, periaortic AT (PeriAo)), beige
347 (subcutaneous (SCAT) and perirenal (PeriRen) AT) and white (pericardiac AT (PeriCard),
348 omentum and gonadal WAT) fat, all associated with different thermogenic capacity, inferred
349 on adipocyte phenotype (**Figure S4d**). While CD226^{high} macrophages were detected in all
350 these tissues, their relative frequency was increased within tissues containing multilocular
351 adipocytes (**Figure 3g**). Furthermore, these cells were efficiently labelled in Retnla^{Cre};
352 R26^{tdTomato} mice (**Figure 3g**). Together, our data indicate that CD226^{high} Retnla^{+} myeloid cells
353 are a unique macrophage subset that is different from conventional dendritic cells, conserved
354 across tissues and enriched in thermogenic adipose depots.
355
356 **CD226^{high} macrophages are regulated by CSF1R and GM-CSF.**
357 We next aimed to identify growth factors regulating CD226^{high} macrophages. We could
358 detect differential expression of *Csf1r* and *Csf2ra* mRNA between CD206^{high} and CD226^{high}
359 macrophages in BAT scRNA-sequencing data [5] (**Figure 4a**), suggesting that these cells might
360 be regulated by different growth factors. Similar observations were made when analyzing
361 peritoneal cavity SCMs and LCMs transcriptomic signatures (Immgen.org) (**Figure S5a**). First,
362 we treated mice with anti-CSF1R blocking Ab (clone AFS98). In BAT, AFS98 administration did
363 not induce a complete macrophage depletion (**Figure 4b**). On the level of macrophage
364 subsets, AFS98 administration decreased the proportions and numbers of BAT CD206^{high}
365 macrophages (**Figures 4c-d**). CD226^{high} cells were also negatively impacted, although at a
366 lower magnitude compared to the CD206^{high} subset (**Figure 4d**) resulting in increased
367 proportions of CD226^{high} cells (**Figure 4c**). Similarly, in the peritoneal cavity AFS98 treatment
368 led to a 70% reduction in LCM numbers while SCM numbers were reduced by 47% indicating
369 a lesser dependence on CSF1R compared to LCMs (**Figure S5b**). Thus, in BAT CD206^{high}
370 macrophages appeared to be the population with the highest dependence on CSF1R
371 signaling.
372 To test whether the reduction of CD226^{high} macrophages induced by AFS98 treatment
373 was cell autonomous or was tied to the disappearance of CD206^{high} macrophages, we
374 generated Retnla^{Cre} x Csf1r$^{fl/fl}$ (Retnla$^{\Delta CSF1R}$) mice. In Retnla$^{\Delta CSF1R}$ mice, we could observe a
375 two-fold reduction of CD226^{high} macrophage numbers in BAT, SCAT, WAT and PW while other
376 populations were unaffected (**Figures 4e and S5c-d**). Yet, this reduction did not align with
377 Retnla^{Cre} efficiency in this population that reached ~85-90% (**Figure 2g**), suggesting that cells
378 remaining in Retnla$^{\Delta CSF1R}$ mice were not CSF1R-dependent.
379 Based on our transcriptomic observations (**Figure 4a**), we next sought to test whether
380 GM-CSF could be regulating CD226^{high} macrophages. CD226^{high} macrophages were recently
381 observed in exocrine glands, in which they were called adenophages and in which they rely
382 on GM-CSF produced by ILC2 [28]. To test whether such a mechanism could be conserved in
383 adipose tissue, we analyzed GM-CSF fate mapping and reporter FROGxAi14 mice that label
384 present (GFP^{+} tdTomato^{+}) and past (GFP^{-} tdTomato^{+}) GM-CSF-producing cells [29]. In WAT,
385 ~25% of CD45^{+} cells were tdTomato^{+} and ~10% were tdTomato^{+} GFP^{+} (**Figure S5e**). Among

386 GFP$^+$ cells, ~75% were ILC2 (**Figure S5h**). To test whether GM-CSF regulated CD226^{high}
387 macrophages, we next analyzed double knock-in/knock-out GM-CSF deficient Csf2^{LacZ}/^{LacZ}
388 (Csf2$^{-/-}$) mice [28]. Similarly to Retnla$^{\Delta CSF1R}$ mice, CD226^{high} macrophages were partially impacted
389 in Csf2$^{-/-}$ mice (**Figure 4f**). Curiously, in peritoneal wash this phenotype was only observed in
390 male Csf2$^{-/-}$ mice (**Figure S5f**).
391 Culturing bone marrow cells *in vitro* with GM-CSF yields both macrophages (GM-Macs)
392 and dendritic cells (GM-DCs) [30]. To test whether the signature of BAT CD226^{high} macrophages
393 overlapped with either GM-CSF-generated cell types, we performed GSEA analysis (**Figures**
394 **4g and S5g**). We found that hallmark genes of BAT CD226^{high} macrophages were mainly
395 expressed in GM-Macs, including *Cd226* and *Fn1* (**Figure 4g**). Similarly, Ly6C^{high} monocytes
396 have been shown to generate "Mo-DCs" upon culture with GM-CSF [31]**.** Again, we found that
397 the BAT CD226^{high} macrophage signature aligned with Mo-DCs rather than Sirpα^+
398 conventional dendritic cells (**Figure 4h**). Although BAT CD226^{high} macrophage signature
399 tended to be regulated when GM-CSF treatment was coupled with IL-4, no statistically
400 significant differences were observed (**Figure S5h**). We repeated such *in vitro* experiments to
401 validate the appearance of CD226^{high} macrophages by flow cytometry. While culturing bone
402 marrow cells with only Csf1 for one week did not favor the generation of these cells, presence
403 of Csf2 triggered development of CD226^{high} macrophages and this phenotype was
404 exacerbated by addition of IL-4 (**Figure 4i**). We then asked whether exposure to these
405 cytokines could skew differentiating macrophages towards the CD226^{high} macrophage
406 phenotype. To test this hypothesis, bone marrow cells were cultured with Csf1 for 4 days,
407 then washed with PBS and cultured for another 3 days in media containing Csf1, Csf2, Csf1 +
408 Csf2, IL-4 or Csf2 + IL-4 (**Figure 4j**). Proportions of CD226^{high} macrophages augmented > 10-
409 fold in presence of Csf2 and IL-4, while other conditions did not trigger such an effect (**Figure**
410 **4j**).
411 BAT macrophages express a clear lipid-associated signature, including *Cd36*, *Fabp4* and
412 *Lpl* [5], with the latter being a core signature gene of CD226^{high} macrophages (**Figures 4g-h**) and
413 of closely-related immature CD206$^-$CD226$^-$*Lpl*^{high} macrophages (**Figure 1a**). GM-CSF-derived
414 macrophages highly expressed these three genes in comparison with their DC counterparts
415 (**Figure 4k**). Since *Cd36*, *Fabp4* and *Lpl* are PPARγ-induced genes, we analyzed their expression
416 in GM-CSF-dependent alveolar macrophages [32] and could confirm significant downregulation
417 in *Pparg*-deficient alveolar macrophages (**Figure 4l**), suggesting that GM-CSF could be
418 regulating CD226^{high} macrophages through PPARγ.
419 Together, our results indicate that IL-4 and several growth factor-dependent pathways,
420 notably GM-CSF and CSF1R-mediated signaling, regulate CD226^{high} macrophages. GM-CSF
421 could regulate CD226^{high} macrophage expression of lipid-associated genes like *Lpl*, *CD36* and
422 *Fabp4*. The partial phenotypes observed in Retnla$^{\Delta CSF1R}$ and Csf2$^{-/-}$ mice could reflect the
423 complementarity of Csf1 and Csf2 observed in vitro (**Figure 4j**), or perhaps the ontogenic
424 heterogeneity of CD226^{high} macrophages (**Figure 2**). Whether M-CSF and GM-CSF differently
425 affect monocyte generation and differentiation depending on their origin remains to be
426 determined.
427
428 **CD226^{high} adipose tissue macrophages regulate lipid metabolism.**
429 We next sought to investigate the role of BAT macrophage subsets on tissue lipid
430 content. To target highly CSF1R-dependent CD206^{high} macrophages, we repeated our AFS98-
431 mediated depletion approach. Mouse body weight and BAT weight tended to decrease in
432 AFS98-injected mice in comparison to isotype controls (**Figure S6a**). AFS98 triggered a well-

433 defined morphological change in BAT with diminished presence of adipocytes with large lipid
434 droplets in comparison to control treated animals (**Figure 5a**). Enzymatic triglyceride (TG)
435 dosage confirmed that BAT TG content was decreased in AFS98 injected mice (**Figure 5b**). Of
436 note, serum TG levels remained similar between both groups of animals (**Figure S6b**). Free
437 fatty acids concentration and diversity were not modified by AFS98 administration (**Figure**
438 **S6c**). These results indicate that CD206^{high} macrophages could support triglyceride storage in
439 BAT, a finding in agreement with recently published results in WAT [9].
440 Since AFS98 treatment could also partly affect CD226^{high} macrophages, we next
441 investigated the role of these cells using Retnla^{Cre} mice. We generated Retnla^{Cre} R26^{DTA} mice
442 (Retnla^{DTA}) to deplete CD226^{high} macrophages across tissues. Blood immune cells were not
443 affected in these mice, indicating the absence of systemic inflammation (**Figure S6d**).
444 However, we could confirm an almost complete absence of BAT Retnla^{+} CD226^{high}
445 macrophages by flow cytometry and confocal microscopy (**Figures 5c-d**). Importantly,
446 CD206^{high} and DN BAT macrophage numbers remained similar between control and Retnla^{DTA}
447 animals (**Figure 5e**). We also noticed the disappearance of CD226^{high} macrophages in all
448 adipose tissue depots that we analyzed (**Figure S6e)**. We also noticed a complete
449 disappearance of SCMs in the peritoneal cavity while LCMs were not affected (**Figure S6f**).
450 Other immune cell types were also unaffected in BAT (**Figure S6g**). Retnla^{DTA} mice are thus
451 appropriate tools to address the function of CD226^{high} macrophages.
452 Depletion of CD226^{high} macrophages triggered a specific BAT phenotype characterized
453 by increased adipocyte droplet size (**Figure 5f**). This was associated with an increased total
454 BAT TG content in Retnla^{DTA} mice when compared to littermate controls, with a particular
455 enrichment of long-chain TGs (**Figure 5g**). We did not detect changes in serum non esterified
456 fatty acids (NEFA) and glucose levels in Retnla^{DTA} mice (**Figure S6h**). However, their serum TG
457 levels were higher than controls while their glycerol levels trended downwards (**Figure 5h**),
458 indicating that CD226^{high} macrophages were regulating triglyceride metabolism.
459
460
461 **Discussion**
462 In the present study, using genetic fate mapping, we demonstrated that a population
463 of blood monocytes is generated independently of GMP-derived cells. We found that these
464 cells are efficiently labelled in Clec9a^{iCre} R26^{TdT} mice suggesting that those monocytes arise
465 mainly from MDPs. Of note, these monocytes preferentially generated CD226^{high}
466 macrophages in adipose tissue and peritoneal cavity, demonstrating the monocyte origin
467 influences their fate. Whether other macrophage subsets also arise mainly from MDPs
468 remains to be established. While the phenotypic distinction between monocytes,
469 macrophages and DCs was challenging for a long time, key findings reported in 2012 by the
470 Immgen consortium solved this problem [33,34]. Macrophages were defined as CD64^{+}MerTK^{+}
471 cells, markers that were not expressed on conventional DCs [33]. We found that CD226^{high}
472 macrophages across tissues displayed a low CD64 expression, challenging the current
473 classification of cells in the macrophage or DC lineage based on these criteria. While BAT
474 CD226^{+} macrophages expressed MerTK and F4/80, supporting their macrophage identity,
475 they also expressed CD11c and MHC-II, two markers traditionally detected and associated
476 with DCs. A key feature of DCs, that is not shared with tissue resident macrophages, is their
477 ability to migrate through the lymphatic vessels to local draining lymph nodes [35]. DC migration
478 via the lymphatic endothelial system depends on a single chemokine receptor, CCR7. Indeed,
479 CCR7 expression allows to discriminate between DCs and macrophages. CD226^{high}

macrophages lack CCR7 expression (data not shown), thus suggesting that these cells cannot migrate through the lymphatic vessels. Furthermore, our data revealed that GMP- and MDP-derived monocytes contribute both to the generation of CD226^{high} macrophages. Therefore, one could expect that depending on their origin, GMP- and MDP-derived CD226^{high} macrophages could display selective functions. Their high MHC-II expression suggests a role in antigen presentation and initiation of adaptive immunity. The ability of GMP- and MDP-derived CD226^{high} macrophages to trigger a T cell response remains to be established.

Previous work on SCMs demonstrated that these cells rely on the transcription factor IRF4 [22]. This study indicated that, independently of their origin, SCMs rely on a unique transcription factor for their survival. However, while only 5% of blood monocytes originate from MDPs, 70% of SCMs arose from these monocytes. Monocytes rely on the chemokine receptor CCR2 for their bone marrow egress and tissue entry [36]. While SCM numbers are reduced in CCR2-deficient mice [22], they are not fully abolished. One could wonder whether MDP-derived monocytes rely solely on CCR2 for bone marrow egress and their subsequent tissue recruitment. Mechanisms governing MDP-derived monocyte bone marrow retention and egress thus require further investigations that are beyond the focus of the present study.

We observed a conserved ratio of Ly6C^{high} : Ly6C^{low} monocytes independently of their origin, suggesting that monocyte conversion occurs at a similar rate in GMP- and MDP-derived monocytes. Yet, our data indicates that GMP- and MDP-derived monocyte fate in tissues depends on their lineage. MDP-derived monocytes are preferentially recruited to specific tissues, i.e. adipose tissues and limb muscle where CD226^{+} macrophages are enriched. A recent study suggests that monocytes locally proliferate upon their tissue recruitment before giving rise to tissue resident macrophage subsets [37]. The proliferative rate of GMP- and MDP-derived monocytes could be significantly different, and this might explain, at least partially, their ability to differentially contribute to specific tissue resident macrophage subsets. The lifespan of GMP- and MDP-derived CD226^{high} macrophages could be an additional factor involved in the aforementioned process.

CD226^{high} macrophages were enriched in adipose tissue and in particular thermogenic depots. Depletion of CD226^{high} macrophages was associated with an increased local and systemic TG content, demonstrating a central role of these cells in lipid metabolism. While CD226^{high} macrophages express several enzymes involved in lipid metabolism [5], how precisely these cells control local and systemic TG content requires further investigations. Previous reports demonstrated that adipose tissue macrophages control lipid storage in a PDGFcc-dependent manner [9]. Of note, mice treated with anti-CSF1R blocking antibody and CCR2$^{-/-}$ mice displayed a different behavior when challenged with high fat diet [9]. While both CD206^{high} and CD226^{high} macrophages show CCR2-dependent monocyte contribution (Figure 1) [5], monocytes mainly contribute to the DN and CD226^{high} subsets. Our data demonstrated that adipose tissue CD206^{+} macrophages showed a higher CSF1R dependency in comparison to DN and CD226^{high} macrophages. Using our scRNA-seq data, we could determine that *Csf1r* expression is higher in CD206^{high} macrophages compared to the CD226^{high} population (data not shown), which could explain the differential impact of AFS98 administration between these two subsets. Whether GMP- and MDP-derived CD226^{+} macrophages rely to a similar extent on CSF1R signaling for their proliferation and renewal needs to be defined. Inversely, CD226^{high} macrophages expressed high levels of *Csf2ra* mRNA compared to CD206^{high} macrophages (data not shown). This observation suggests that GM-CSF signaling plays a role in the maintenance of CD226^{high} macrophages.

In the present study, we identify CD226^{high} macrophages as a new myeloid subset bearing features of both macrophages (F4/80^{+} MerTK^{+}) and dendritic cells (CD64^{low} CD11c^{+} MHC-II^{high}), that is conserved across tissues. Similar findings were reported in a recent study comparing murine and human peritoneal cells [24]. Indeed, the human counterpart to murine CD226^{high} SCMs appeared to be CD14^{+} cells that also express the DC marker CD1c [24]. Importantly, this observation indicates that CD226^{high} cells described herein are conserved in humans. We detected a similar population in human white adipose tissue (Human Single Cell Atlas from the Broad Institute, data not shown), indicating that these cells are also conserved across several tissues in humans. This work paves the way to define the relative role of GMP- and MDP-derived monocytes during infections, acute and chronic (obesity, atherosclerosis…) inflammatory diseases and cancer development.

Acknowledgments

We thank the C3M Animal facility, and the C3M Flow Cytometry Core Facility financed by Conseil Général CG06 and Conseil Régional PACA. We thank Dr. Florent Ginhoux for sharing genetic mouse models. We thank Sandrine Quemener (Lille Pasteur Institute) for technical assistance. SI is funded by Institut National de la Sante et de la Recherche Medicale (INSERM) and Agence Nationale de la Recherche (ANR-22-CE14-0027-02; ANR-21-CE15-0020-02; ANR-23-CE14-0054-02; ANR-23-CE15-0032-01). JWW was supported by NIH R01AI165553. MC was supported by NIH T32 HL166142. AG was supported by the French government through the France 2030 investment plan managed by the National Research Agency (ANR), as part of the Initiative of Excellence Université Côte d'Azur under reference number ANR- 15-IDEX-01. EM was funded by the Deutsche Forschungsgemeinschaft (DFG, German Research Foundation) under Germany's Excellence Strategy-EXC2151-390873048, SFB1454 (Project number 432325352), and FOR5547 – Project-ID 503306912.

Author contribution

AG and SI designed the study. AG and SI wrote the manuscript and prepared the figures with input from all co-authors. AG, ZC, FW, ST, SG, MT, AC, LL, KA, LL, MG, TP, SF, MC, BD, EG, MF, EB, ZM, FNZ, JGN, JWW, AB and SI performed experiments. AG, ZC, FW, ST, MT, KA, SG, TP, JWW, DM, MNA, AB and SI analyzed data. EM, DV, MM, JH, DD and BB provided tools and expertise. SI obtained funding for the project.

Conflicts of interest

The authors declare no competing interests.

Methods

Experimental models

Mouse models

Wild-type C57BL/6J (Jax #000664), CX3CR1^{gfp} (B6.Cg-Ptprca Cx3cr1$^{tm1Litt/LittJ}$, Jax #008451), Ms4a3^{cre} (C57BL/6J-Ms4a3$^{em2(cre)Fgnx}$/J, Jax #036382), R26$^{LSL\text{-}tdTomato}$ (B6.Cg-Gt(ROSA)26Sor$^{tm9(CAG\text{-}tdTomato)Hze}$/J, Jax#007909), Clec9a^{icre} (B6J.B6N(Cg)-Clec9a$^{tm2.1(icre)Crs}$/J, Jax#025523), CD45.1 (B6.SJL-Ptprc^{a} Pepc^{b}/BoyJ, Jax# 002014) and R26$^{LSL\text{-}DTA}$ (B6.129P2-Gt(ROSA)26Sor$^{tm1(DTA)Lky}$/J, Jax# 009669) mice used in this study were maintained under C57BL/6J background and originally purchased from Jax Labs. CCR2$^{cre/ERT2}$ (C57BL/6NTac-Ccr2$^{tm2982(T2A\text{-}Cre7ESR1\text{-}T2A\text{-}mKate2)}$) [38] and Csf2$^{-/-}$ [28] mice were provided by Dr. Burkhard Becher.

573 Ms4a3$^{cre/ERT2}$ mice[3] were provided by Dr. Florent Ginhoux. Retnla^{cre} mice[27] were provided by
574 Dr. David Voehringer. Tnfrsf11a^{Cre}; Rosa26$^{LSL-YFP}$ and Ms4a3^{FlpO}; Rosa26$^{FSF-tdTomato}$ mice[18] were
575 provided by Dr. Elvira Mass. Experimental and control animals were co-housed, and
576 littermate controls were used as often as possible. Mice were bred and housed in certified
577 housing facilities with an ambient temperature of ~20-23 °C, a 12/12-hour light/dark cycle
578 and food available ad libitum. Animals were euthanized by cervical dislocation. Animal
579 protocols required for experimentation other than organ collection were authorized by the
580 French Ministry of Higher Education and Research upon approval of the local ethical
581 committee (CIEPAL Azur) at Université Côte d'Azur, and by the Institutional Animal Care and
582 Use Committee (IACUC) at University of Minnesota Medical School.
583
584 ***In vivo* treatments**
585 Administration of tamoxifen
586 CCR2^{creERT2} x R26^{TdTomato} mice were treated with tamoxifen dissolved in corn oil (20 mg/mL)
587 by a single oral gavage (250 μL/mouse). Animals were sacrificed 2 days later and assessed for
588 labeling efficiency in brown adipose tissue by flow cytometry.
589 CX3CR1^{creERT2} x R26^{TdTomato} mice were injected intra-peritoneally with 10 mg/mL tamoxifen
590 (200 μL per mouse in 10% EtOH and sunflower oil) daily for 5 days. Labelling efficiency was
591 assessed in brain, blood and brown adipose tissue for each experiment involving this strain.
592 Ms4a3^{creERT2} x R26^{TdTomato} mice were treated with tamoxifen dissolved in corn oil (20 mg/mL)
593 by oral gavage (100 μL/mouse) daily for 5 days. Labelling efficiency was assessed in blood and
594 brown adipose tissue 3, 10 and 17 days following the last tamoxifen administration.
595 Monocyte depletion with MC-21
596 Mice were injected intra-peritoneally once a day for 1, 2 or 5 days with 10 µg MC-21 (anti-
597 CCR2) antibody or vehicle (PBS) and were sacrificed 16 h after the last injection for analysis
598 of brown adipose tissue macrophages. Monocyte depletion efficiency was confirmed by
599 blood analysis.
600 Macrophage depletion with AFS98
601 Mice were injected intra-peritoneally twice (48 hours apart) with 500 µg anti-CD115 blocking
602 antibody (AFS98, BioXCell cat#BE0213) or isotype control (Rat IgG2a, BioXcell cat#BE0089)
603 and were sacrificed 16 h after the last injection for analysis of adipose tissue macrophages.
604
605 ***In vitro culture***
606 Total bone marrow cells were isolated by flushing bone marrow out of femurs and tibias using
607 PBS. Bone marrow cells were cultured in RPMI medium containing 10% FBS, 2mM L-
608 Glutamine, 50U/mL Penicillin and 50 µg/mL Streptomycin. Growth factors and cytokines were
609 added as indicated in figure legends, at a concentration of 50 ng/mL (M-CSF, GM-CSF) or
610 10ng/mL (IL-4).
611
612 ***Flow cytometry***
613 Tissues were harvested after cervical dislocation and washed in PBS. Splenocytes were
614 prepared by gently crushing the spleen on a 70 μm strainer in flow buffer (PBS containing 1%
615 BSA and 2 mM EDTA). Peritoneal cells were obtained by performing lavage with 5 mL PBS.
616 Bone marrow cells were prepared by flushing femurs and tibias with flow buffer. Adipose
617 depots, lungs, liver and brains were harvested, minced with scissors, and then incubated for
618 45 min with PBS containing 3 mg/mL collagenase A and 100µg/mL DNAse I at 37 °C. For
619 experiments with Tnfrsf11a^{Cre}-Ms4a3^{Flp} double fate-mapper mice, adipose tissues were

620 incubated for 30 min with PBS containing 0.5% BSA, 2 mg/mL Collagenase-II and 2.5 mM
621 $CaCl_2$. Digested tissues were then homogenized using a 1 mL syringe with a 20G needle and
622 passed through a 70 µm strainer. Brain immune cells were further enriched using a Percoll
623 gradient. Blood was drawn from the submandibular vein and collected in heparinized tubes
624 or Eppendorf tubes containing 15 µl 500 mM EDTA. Red blood cells were lysed using BD
625 Pharm Lyse lysing solution (BdBiosciences cat #555899). Cells were washed with flow buffer
626 and then surface stained. All antibodies were used 1/200. A list of all antibodies used in
627 provided in Supplementary Table 1. Flow cytometry data were acquired using a BD FACS
628 Canto II, BD FACSymphony A5 and a Cytek Aurora cytometer with 5 laser configuration. All
629 analyses were performed using FlowJo software (Tree Star).
630
631 ***Metabolite analyses***
632 Colorimetric quantification of metabolites
633 Glycerol, TG and NEFA contents were measured from serum. Free glycerol reagent and
634 standard were used according to the manufacturer's protocol. NEFA-HR2 R1 + R2 FUJIFILM
635 were used according to the manufacturer's protocol.
636
637 Serum lipidomic analysis by GCMS-NCI
638 Materials: Fatty acid calibration standards and deuterated fatty acid internal standards
639 (saturated and unsaturated) were purchased from CDN Isotopes (Cluzeau Info Lab, Sainte Foy
640 La Grande, France) and Cayman (Bertin Pharma, Montigny-le-Bretonneux, France)
641 respectively. Chemicals of the highest grade available were from Sigma Aldrich (Saint-Quentin
642 Fallavier, France). LCMSMS quality grade solvents were purchased from Fischer Scientific
643 (Illkirch, France).
644 Methods: Serum (25µL) was mixed with 5 µL of a fatty acid internal standard mix, containing
645 260 ng of myristic acid-d3, 1128 ng of palmitic acid-d3, 840 ng of stearic acid-d3, 720 ng of
646 linoleic acid d4, 10.4 ng of arachidic acid-d3, 432 ng of arachidonic acid-d8, 10.8 ng of behenic
647 acid-d3, 108 ng of DHA-d5, 5.2 ng of Lignoceric-d4, and 4 ng of cerotic acid-d4. To separate
648 non-esterified fatty acids, the spiked serum samples were mixed with 1.2ml of Dole's reagent
649 (Isopropanol/Hexane/Phosphoric acid 2M 40/10/1 v/v/v). Free fatty acids were then
650 recovered with 1 ml of hexane and 1 ml of distilled water. The organic phase was collected
651 and evaporated under vacuum. Fatty acids were then analyzed as pentafluorobenzyl esters
652 (PFB-FAs esters) by NCI-GCMS as previously described [39]. Calibration curves were obtained
653 using myristic acid (0.05 - 0.8 µg), palmitic acid (1 - 8 µg), stearic acid (0.5 – 2 µg), linoleic acid
654 (2 - 8 µg), arachidic acid (0.01 – 0.04 µg), arachidonic acid (1 - 4 µg), docosahexaenoic acid
655 (0.4 – 1.6 µg), and docosapentaenoic acid (0.1 – 0.4 µg) extracted by the same method used
656 for plasma. The abundances of serum free fatty acids were determined by negative chemical
657 ionization mode (NCI) GCMS. Linear regression was applied for calculations.
658
659 Quantitative analysis of brown adipose tissues by targeted mass spectrometry
660 Materials: Glyceride standards, (17:0)2-d5 DG and (17:0)3 TG were obtained from Avanti
661 Polar Lipids (Coger SAS, Paris, France). High-grade organic solvent modifiers were purchased
662 from Sigma Aldrich (Saint-Quentin Fallavier, France). LC-MSMS quality grade solvents were
663 purchased from Fischer Scientific (Illkirch, France).
664 Preparation of lipid extracts: Gravimetrically weighed adipose tissues suspended in
665 $CHCl_3$:MeOH (2:1) were homogenized with the Omni Bead Ruptor 24 (Omni International.
666 Inc.) coupled to a RT400 savant condensation trap (Thermo Scientific). DG (1µg) and TG

667 (2.5µg) internal standards were added to approximately 0.5mg of adipose tissue
668 homogenates. The spiked homogenates were vortexed, centrifuged, collected into inserts,
669 dried under vacuum, and resuspended in 100µl of $CHCl_3$:MeOH (2:1).
670 Analysis of Glycerides by UHPLC-MS^2: The homogenates (3 µL) were analyzed by LC-MSMS.
671 For the separation and elution of analytes, a Nucleodur ISIS C18 1,8 µm guard (3 x 4mm) and
672 analytical (3 x 100mm) column (Marechey-Nagel, Hoerdt Cedex, France) maintained at 50°C
673 were used[40]. Briefly, DG and TG were resolved on a 1260 Infinity LC system (Agilent
674 Technologies) with a gradient of mobile phase A (acetonitrile/water/1M ammonium formate
675 (60/39/1 v/v/v) with 0.1% formic acid), and mobile phase B (isopropanol/acetonitrile/1M
676 ammonium formate (90/9/1 v/v/v) with 0.1% formic acid)[41] at a flow rate of 0.45ml/min set
677 as follows : 1 min hold at 30% B; 30-60% B in 2 min; 60-72% B in 15 min; 72-99% B in 20min;
678 3 min hold at 99%, 99%-30% ramp-down in 0.1 min and, maintained at 30% B for 3.9 min.
679 Acquisition was realized on a 6460 Triple Quadrupole (Agilent Technologies) equipped with
680 an ESI Jet stream source (temperature 150 °C, nebulizer 15 L/min, sheath gas 11 L/min, sheath
681 gas temperature 150°C, capillary 4500 V and nozzle voltage 1200 V) operated in positive
682 Single Reaction Monitoring (SRM) mode (fragmentor 152 and 220 V, collision energy 29 and
683 25 V for DG and TG respectively. Ammoniated DG were quantified according to the response
684 observed from the neutral loss of either their sn-1 or sn-2 fatty acid. Ammoniated TG were
685 quantified according to the sum of the responses resulting from the neutral loss of either their
686 sn-1, sn-2, and sn-3 fatty acids. Finally, lipid concentrations were determined by calculating
687 the relative response of each lipiform to its respective internal standard.
688
689 ***Histology and immunostaining***
690 Tissues were harvested and fixed for 4 h at room temperature or overnight at 4°C in ADAPT-
691 3D fixative [42] (4% paraformaldehyde solution with 30% sucrose, pH9). Samples were then
692 washed in 1X PBS. For tissue sections, a paraffin infiltration was performed on dehydrated
693 tissues (Myr Spin Tissue Processor STP 120). Then, tissues were embedded in paraffin
694 (inclusion center EC350-B&PMP). 7 µm sections were performed using a HM340E microtome
695 (Microm Microtech, Francheville France). Paraffin sections were then de-paraffinized and
696 stained using hematoxylin & eosin. For whole mount microscopy, tissues were decolored and
697 stained following the ADAPT-3D method [42] and cleared in ethyl cinnamate. Images were
698 acquired on a Nikon CSU-W1 spinning disk microscope.
699
700 ***Single-cell RNA-seq integration***
701 Single-cell datasets were downloaded from GEO database: GSE177635 [5] (brown fat tissue, WT
702 sample GSM5378577); GSE203097 [23] (adrenal gland tissue, samples: GSM6153750 and
703 GSM6153751); GSE225665 [43] (peritoneal wash, samples: GSM7053956 and GSM7053957).
704 For splenic tissue [25], single-cell dataset was downloaded from
705 https://figshare.com/articles/dataset/Bulk_and_single-cell_RNA-seq_data/22232056/1. Cell
706 type annotations were used from original studies (for brown fat and adrenal gland datasets -
707 provided by authors, for peritoneal wash and spleen datasets downloaded together with data
708 from public resources). Datasets were subsetted to maintain only monocyte, macrophage,
709 and dendritic cell populations.
710 Datasets were integrated using Seurat v4.3.0 tool[44] using RPCA approach. Samples, coming
711 from different datasets were log normalized, and 3000 variable features were selected using
712 'vst' method. After the selection of integration features, highly variable genes were scaled
713 and variation coming from the percentage of mitochondrial genes and number of counts were

714 regressed out. Integration anchors were found with no k.filter and 250 n.trees parameters.
715 Integrated data were scaled and the final umap reduction was calculated based on the first
716 25 PCA components.
717 For DC3 signature enrichment, the top 100 differentially expressed genes were calculated
718 using the FindMarkers function, with the following parameters: logfc.threshold = 0.01,
719 min.pct = 0.01, only.pos = T. Enrichment plot was created using
720 plotCoregulationProfileReduction function from fgsea package v1.27.1[45].
721 Scatter plots were visualized using ggplot2 v3.4.2 package[46]. Shapes of cluster borders were
722 calculated by first estimating 2d kernel density using MASS package v7.3-58.4[47], followed by
723 creating a grid graph with igraph package v1.4.3[48] and calculating α-shape of clusters using
724 alphahull v2.5 package[49]. Visualization of gene expression for Gallerand et al., 2021 dataset
725 in Figures S1, and S4 was generated using scNavigator (Artyomov lab,
726 https://artyomovlab.wustl.edu/scn/).
727
728 ***Statistical Analysis***
729 All data are represented in mean ± SEM. Statistical analysis was performed with GraphPad
730 Prism 10 as indicated in each figure legend. Presence of statistically significant differences
731 between conditions are indicated as follows: ns $p>0.05$; * $p<0.05$; ** $p<0.01$; *** $p<0.001$;
732 **** $p<0.0001$.
733
734
735 **References**
736

737 1. Mass, E., Nimmerjahn, F., Kierdorf, K., and Schlitzer, A. (2023). Tissue-specific
738 macrophages: how they develop and choreograph tissue biology. Nat. Rev. Immunol.
739 *23*, 563–579. 10.1038/s41577-023-00848-y.
740 2. Ginhoux, F., and Guilliams, M. (2016). Tissue-Resident Macrophage Ontogeny and
741 Homeostasis. Immunity *44*, 439–449. 10.1016/j.immuni.2016.02.024.
742 3. Liu, Z., Gu, Y., Chakarov, S., Bleriot, C., Kwok, I., Chen, X., Shin, A., Huang, W., Dress,
743 R.J., Dutertre, C.A., et al. (2019). Fate Mapping via Ms4a3-Expression History Traces
744 Monocyte-Derived Cells. Cell *178*, 1509–1525 e1519. 10.1016/j.cell.2019.08.009.
745 4. Félix, I., Ollikainen, J., Haque, A., Karhula, J., Salmi, M., Jokela, H., and Rantakari, P.
746 (2025). Embryonic macrophages in brown adipose tissue are spatially associated
747 with developing nerves. bioRxiv, 2025.2001.2016.632922.
748 10.1101/2025.01.16.632922.
749 5. Gallerand, A., Stunault, M.I., Merlin, J., Luehmann, H.P., Sultan, D.H., Firulyova,
750 M.M., Magnone, V., Khedher, N., Jalil, A., Dolfi, B., et al. (2021). Brown adipose tissue
751 monocytes support tissue expansion. Nat Commun *12*, 5255. 10.1038/s41467-021-
752 25616-1.
753 6. Rosen, E.D., and Spiegelman, B.M. (2014). What we talk about when we talk about
754 fat. Cell *156*, 20–44. 10.1016/j.cell.2013.12.012.
755 7. Nicholls, D.G. (2017). The hunt for the molecular mechanism of brown fat
756 thermogenesis. Biochimie *134*, 9–18. 10.1016/j.biochi.2016.09.003.
757 8. Wolf, Y., Boura-Halfon, S., Cortese, N., Haimon, Z., Sar Shalom, H., Kuperman, Y.,
758 Kalchenko, V., Brandis, A., David, E., Segal-Hayoun, Y., et al. (2017). Brown-adipose-
759 tissue macrophages control tissue innervation and homeostatic energy expenditure.
760 Nat Immunol *18*, 665–674. 10.1038/ni.3746.

761 9. Cox, N., Crozet, L., Holtman, I.R., Loyher, P.L., Lazarov, T., White, J.B., Mass, E.,
762 Stanley, E.R., Elemento, O., Glass, C.K., and Geissmann, F. (2021). Diet-regulated
763 production of PDGFcc by macrophages controls energy storage. Science *373*.
764 10.1126/science.abe9383.
765 10. Ingersoll, M.A., Spanbroek, R., Lottaz, C., Gautier, E.L., Frankenberger, M., Hoffmann,
766 R., Lang, R., Haniffa, M., Collin, M., Tacke, F., et al. (2010). Comparison of gene
767 expression profiles between human and mouse monocyte subsets. Blood *115*, e10–
768 19. 10.1182/blood-2009-07-235028.
769 11. Sunderkotter, C., Nikolic, T., Dillon, M.J., Van Rooijen, N., Stehling, M., Drevets, D.A.,
770 and Leenen, P.J. (2004). Subpopulations of mouse blood monocytes differ in
771 maturation stage and inflammatory response. J Immunol *172*, 4410–4417.
772 10.4049/jimmunol.172.7.4410.
773 12. Carlin, L.M., Stamatiades, E.G., Auffray, C., Hanna, R.N., Glover, L., Vizcay-Barrena,
774 G., Hedrick, C.C., Cook, H.T., Diebold, S., and Geissmann, F. (2013). Nr4a1-dependent
775 Ly6C(low) monocytes monitor endothelial cells and orchestrate their disposal. Cell
776 *153*, 362–375. 10.1016/j.cell.2013.03.010.
777 13. Auffray, C., Fogg, D., Garfa, M., Elain, G., Join-Lambert, O., Kayal, S., Sarnacki, S.,
778 Cumano, A., Lauvau, G., and Geissmann, F. (2007). Monitoring of blood vessels and
779 tissues by a population of monocytes with patrolling behavior. Science *317*, 666–
780 670. 10.1126/science.1142883.
781 14. Hanna, R.N., Cekic, C., Sag, D., Tacke, R., Thomas, G.D., Nowyhed, H., Herrley, E.,
782 Rasquinha, N., McArdle, S., Wu, R., et al. (2015). Patrolling monocytes control tumor
783 metastasis to the lung. Science *350*, 985–990. 10.1126/science.aac9407.
784 15. Trzebanski, S., Kim, J.S., Larossi, N., Raanan, A., Kancheva, D., Bastos, J., Haddad, M.,
785 Solomon, A., Sivan, E., Aizik, D., et al. (2024). Classical monocyte ontogeny dictates
786 their functions and fates as tissue macrophages. Immunity.
787 10.1016/j.immuni.2024.04.019.
788 16. Menezes, S., Melandri, D., Anselmi, G., Perchet, T., Loschko, J., Dubrot, J., Patel, R.,
789 Gautier, E.L., Hugues, S., Longhi, M.P., et al. (2016). The Heterogeneity of Ly6C(hi)
790 Monocytes Controls Their Differentiation into iNOS(+) Macrophages or Monocyte-
791 Derived Dendritic Cells. Immunity *45*, 1205–1218. 10.1016/j.immuni.2016.12.001.
792 17. Jung, S., Aliberti, J., Graemmel, P., Sunshine, M.J., Kreutzberg, G.W., Sher, A., and
793 Littman, D.R. (2000). Analysis of fractalkine receptor CX(3)CR1 function by targeted
794 deletion and green fluorescent protein reporter gene insertion. Mol Cell Biol *20*,
795 4106–4114. 10.1128/MCB.20.11.4106-4114.2000.
796 18. Huang, H., Balzer, N.R., Seep, L., Splichalova, I., Blank-Stein, N., Viola, M.F., Franco
797 Taveras, E., Acil, K., Fink, D., Petrovic, F., et al. (2025). Kupffer cell programming by
798 maternal obesity triggers fatty liver disease. Nature. 10.1038/s41586-025-09190-w.
799 19. Mass, E., Ballesteros, I., Farlik, M., Halbritter, F., Gunther, P., Crozet, L., Jacome-
800 Galarza, C.E., Handler, K., Klughammer, J., Kobayashi, Y., et al. (2016). Specification
801 of tissue-resident macrophages during organogenesis. Science *353*.
802 10.1126/science.aaf4238.
803 20. Mack, M., Cihak, J., Simonis, C., Luckow, B., Proudfoot, A.E., Plachy, J., Bruhl, H.,
804 Frink, M., Anders, H.J., Vielhauer, V., et al. (2001). Expression and characterization of
805 the chemokine receptors CCR2 and CCR5 in mice. J. Immunol. *166*, 4697–4704.
806 10.4049/jimmunol.166.7.4697.

807 21. Schraml, B.U., van Blijswijk, J., Zelenay, S., Whitney, P.G., Filby, A., Acton, S.E.,
808 Rogers, N.C., Moncaut, N., Carvajal, J.J., and Reis e Sousa, C. (2013). Genetic tracing
809 via DNGR-1 expression history defines dendritic cells as a hematopoietic lineage. Cell
810 *154*, 843–858. 10.1016/j.cell.2013.07.014.
811 22. Kim, K.W., Williams, J.W., Wang, Y.T., Ivanov, S., Gilfillan, S., Colonna, M., Virgin,
812 H.W., Gautier, E.L., and Randolph, G.J. (2016). MHC II+ resident peritoneal and
813 pleural macrophages rely on IRF4 for development from circulating monocytes. J Exp
814 Med *213*, 1951–1959. 10.1084/jem.20160486.
815 23. Dolfi, B., Gallerand, A., Firulyova, M.M., Xu, Y., Merlin, J., Dumont, A., Castiglione, A.,
816 Vaillant, N., Quemener, S., Gerke, H., et al. (2022). Unravelling the sex-specific
817 diversity and functions of adrenal gland macrophages. Cell Rep. *39*, 110949.
818 10.1016/j.celrep.2022.110949.
819 24. Han, J., Gallerand, A., Erlich, E.C., Helmink, B.A., Mair, I., Li, X., Eckhouse, S.R., Dimou,
820 F.M., Shakhsheer, B.A., Phelps, H.M., et al. (2024). Human serous cavity
821 macrophages and dendritic cells possess counterparts in the mouse with a distinct
822 distribution between species. Nat. Immunol. *25*, 155–165. 10.1038/s41590-023-
823 01688-7.
824 25. Liu, Z., Wang, H., Li, Z., Dress, R.J., Zhu, Y., Zhang, S., De Feo, D., Kong, W.T., Cai, P.,
825 Shin, A., et al. (2023). Dendritic cell type 3 arises from Ly6C(+) monocyte-dendritic
826 cell progenitors. Immunity *56*, 1761–1777 e1766. 10.1016/j.immuni.2023.07.001.
827 26. Tabula Muris, C. (2020). A single-cell transcriptomic atlas characterizes ageing tissues
828 in the mouse. Nature *583*, 590–595. 10.1038/s41586-020-2496-1.
829 27. Krljanac, B., Schubart, C., Naumann, R., Wirtz, S., Culemann, S., Kronke, G., and
830 Voehringer, D. (2019). RELMalpha-expressing macrophages protect against fatal lung
831 damage and reduce parasite burden during helminth infection. Sci Immunol *4*.
832 10.1126/sciimmunol.aau3814.
833 28. Westermann, F., Tuzlak, S., Kreiner, V., Bejarano, D., Bijnen, M., Cecconi, V., van
834 Hove, H., Wang, H., Litscher, G., Ignacio, A., et al. (2024). Unveiling a unique
835 macrophage population in exocrine glands sustained by ILC2-derived GM-CSF.
836 bioRxiv, 2024.2010.2030.620897. 10.1101/2024.10.30.620897.
837 29. Komuczki, J., Tuzlak, S., Friebel, E., Hartwig, T., Spath, S., Rosenstiel, P., Waisman, A.,
838 Opitz, L., Oukka, M., Schreiner, B., et al. (2019). Fate-Mapping of GM-CSF Expression
839 Identifies a Discrete Subset of Inflammation-Driving T Helper Cells Regulated by
840 Cytokines IL-23 and IL-1beta. Immunity *50*, 1289–1304 e1286.
841 10.1016/j.immuni.2019.04.006.
842 30. Helft, J., Bottcher, J., Chakravarty, P., Zelenay, S., Huotari, J., Schraml, B.U., Goubau,
843 D., and Reis e Sousa, C. (2015). GM-CSF Mouse Bone Marrow Cultures Comprise a
844 Heterogeneous Population of CD11c(+)MHCII(+) Macrophages and Dendritic Cells.
845 Immunity *42*, 1197–1211. 10.1016/j.immuni.2015.05.018.
846 31. Briseno, C.G., Haldar, M., Kretzer, N.M., Wu, X., Theisen, D.J., Kc, W., Durai, V.,
847 Grajales-Reyes, G.E., Iwata, A., Bagadia, P., et al. (2016). Distinct Transcriptional
848 Programs Control Cross-Priming in Classical and Monocyte-Derived Dendritic Cells.
849 Cell Rep. *15*, 2462–2474. 10.1016/j.celrep.2016.05.025.
850 32. Schneider, C., Nobs, S.P., Kurrer, M., Rehrauer, H., Thiele, C., and Kopf, M. (2014).
851 Induction of the nuclear receptor PPAR-gamma by the cytokine GM-CSF is critical for
852 the differentiation of fetal monocytes into alveolar macrophages. Nat. Immunol. *15*,
853 1026–1037. 10.1038/ni.3005.

854 33. Gautier, E.L., Shay, T., Miller, J., Greter, M., Jakubzick, C., Ivanov, S., Helft, J., Chow,
855 A., Elpek, K.G., Gordonov, S., et al. (2012). Gene-expression profiles and
856 transcriptional regulatory pathways that underlie the identity and diversity of mouse
857 tissue macrophages. Nat Immunol *13*, 1118–1128. 10.1038/ni.2419.
858 34. Miller, J.C., Brown, B.D., Shay, T., Gautier, E.L., Jojic, V., Cohain, A., Pandey, G.,
859 Leboeuf, M., Elpek, K.G., Helft, J., et al. (2012). Deciphering the transcriptional
860 network of the dendritic cell lineage. Nat. Immunol. *13*, 888–899. 10.1038/ni.2370.
861 35. Randolph, G.J., Ivanov, S., Zinselmeyer, B.H., and Scallan, J.P. (2017). The Lymphatic
862 System: Integral Roles in Immunity. Annu. Rev. Immunol. *35*, 31–52.
863 10.1146/annurev-immunol-041015-055354.
864 36. Serbina, N.V., and Pamer, E.G. (2006). Monocyte emigration from bone marrow
865 during bacterial infection requires signals mediated by chemokine receptor CCR2.
866 Nat. Immunol. *7*, 311–317. 10.1038/ni1309.
867 37. Vanneste, D., Bai, Q., Hasan, S., Peng, W., Pirottin, D., Schyns, J., Marechal, P.,
868 Ruscitti, C., Meunier, M., Liu, Z., et al. (2023). MafB-restricted local monocyte
869 proliferation precedes lung interstitial macrophage differentiation. Nat. Immunol.
870 *24*, 827–840. 10.1038/s41590-023-01468-3.
871 38. Croxford, A.L., Lanzinger, M., Hartmann, F.J., Schreiner, B., Mair, F., Pelczar, P.,
872 Clausen, B.E., Jung, S., Greter, M., and Becher, B. (2015). The Cytokine GM-CSF
873 Drives the Inflammatory Signature of CCR2+ Monocytes and Licenses Autoimmunity.
874 Immunity *43*, 502–514. 10.1016/j.immuni.2015.08.010.
875 39. Nguyen, M., Bourredjem, A., Piroth, L., Bouhemad, B., Jalil, A., Pallot, G., Le Guern,
876 N., Thomas, C., Pilot, T., Bergas, V., et al. (2021). High plasma concentration of non-
877 esterified polyunsaturated fatty acids is a specific feature of severe COVID-19
878 pneumonia. Sci. Rep. *11*, 10824. 10.1038/s41598-021-90362-9.
879 40. Tamba Sompila, A.W., Heron, S., Hmida, D., and Tchapla, A. (2017). Fast non-
880 aqueous reversed-phase liquid chromatography separation of triacylglycerol
881 regioisomers with isocratic mobile phase. Application to different oils and fats. J.
882 Chromatogr. B Analyt. Technol. Biomed. Life Sci. *1041-1042*, 151–157.
883 10.1016/j.jchromb.2016.12.030.
884 41. Cajka, T., Hricko, J., Rudl Kulhava, L., Paucova, M., Novakova, M., and Kuda, O.
885 (2023). Optimization of Mobile Phase Modifiers for Fast LC-MS-Based Untargeted
886 Metabolomics and Lipidomics. Int. J. Mol. Sci. *24*. 10.3390/ijms24031987.
887 42. Daniel D. Lee, D.L.D., Leon C.D. Smyth et al. (2025). ADAPT-3D: Accelerated Deep
888 Adaptable Processing of Tissue for 3-Dimensional Fluorescence Tissue Imaging for
889 Research and Clinical Settings. PREPRINT (Version 1) available at Research Square.
890 [https://doi.org/10.21203/rs.3.rs-6109657/v1].
891 43. Li, X., Mara, A.B., Musial, S.C., Kolling, F.W., Gibbings, S.L., Gerebtsov, N., and
892 Jakubzick, C.V. (2024). Coordinated chemokine expression defines macrophage
893 subsets across tissues. Nat. Immunol. *25*, 1110–1122. 10.1038/s41590-024-01826-9.
894 44. Hao, Y., Hao, S., Andersen-Nissen, E., Mauck, W.M., 3rd, Zheng, S., Butler, A., Lee,
895 M.J., Wilk, A.J., Darby, C., Zager, M., et al. (2021). Integrated analysis of multimodal
896 single-cell data. Cell *184*, 3573–3587 e3529. 10.1016/j.cell.2021.04.048.
897 45. Korotkevich, G., Sukhov, V., Budin, N., Shpak, B., Artyomov, M.N., and Sergushichev,
898 A. (2021). Fast gene set enrichment analysis. bioRxiv, 060012. 10.1101/060012.
899 46. Wickham, H. (2016). ggplot2: Elegant Graphics for Data Analysis. Springer-Verlag
900 New York *978-3-319-24277-4*.

47. Venables WN, R.B. (2002). Modern Applied Statistics with S, Fourth edition. Springer, New York *ISBN 0-387-95457-0*.
48. Csárdi G, N.T., Traag V, Horvát S, Zanini F, Noom D, Müller K (2024). igraph: Network Analysis and Visualization in R. *R package version 2.0.3*. doi:10.5281/zenodo.7682609.
49. Pateiro-López, B., & Rodríguez-Casal, A (2010). Generalizing the Convex Hull of a Sample: The R Package alphahull. Journal of Statistical Software *34(5), 1–28*.

Figure 1

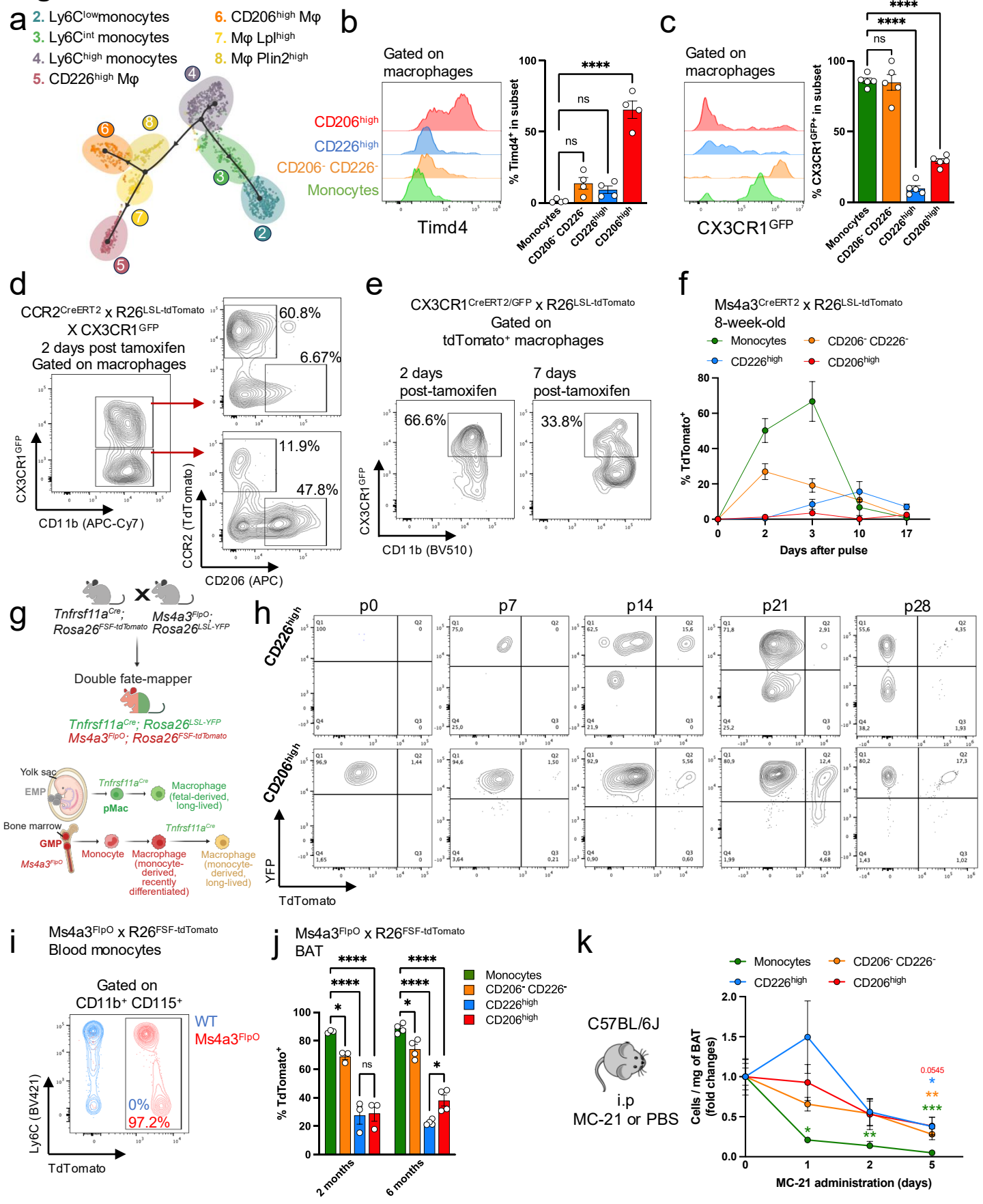
a
2. Ly6C^low monocytes
3. Ly6C^int monocytes
4. Ly6C^high monocytes
5. CD226^high Mφ
6. CD206^high Mφ
7. Mφ Lpl^high
8. Mφ Plin2^high
b
Gated on macrophages
CD206^high
CD226^high
CD206⁻ CD226⁻
Monocytes
Timd4
% Timd4⁺ in subset
****
ns
ns
Monocytes
CD206⁻ CD226⁻
CD226^high
CD206^high
c
Gated on macrophages
CX3CR1^GFP
% CX3CR1^GFP⁺ in subset
****
****
ns
d
CCR2^CreERT2 x R26^LSL-tdTomato
X CX3CR1^GFP
2 days post tamoxifen
Gated on macrophages
60.8%
6.67%
11.9%
47.8%
CX3CR1^GFP
CD11b (APC-Cy7)
CCR2 (TdTomato)
CD206 (APC)
e
CX3CR1^CreERT2/GFP x R26^LSL-tdTomato
Gated on
tdTomato⁺ macrophages
2 days
post-tamoxifen
7 days
post-tamoxifen
66.6%
33.8%
CX3CR1^GFP
CD11b (BV510)
f
Ms4a3^CreERT2 x R26^LSL-tdTomato
8-week-old
Monocytes
CD206⁻ CD226⁻
CD226^high
CD206^high
% TdTomato⁺
Days after pulse
g
Tnfrsf11a^Cre; Rosa26^FSF-tdTomato
Ms4a3^FlpO; Rosa26^LSL-YFP
Double fate-mapper
Tnfrsf11a^Cre; Rosa26^LSL-YFP
Ms4a3^FlpO; Rosa26^FSF-tdTomato
Yolk sac
EMP
pMac
Macrophage (fetal-derived, long-lived)
Bone marrow
GMP
Ms4a3^FlpO
Monocyte
Macrophage (monocyte-derived, recently differentiated)
Macrophage (monocyte-derived, long-lived)
h
p0
p7
p14
p21
p28
CD226^high
CD206^high
YFP
TdTomato
i
Ms4a3^FlpO x R26^FSF-tdTomato
Blood monocytes
Gated on
CD11b⁺ CD115⁺
WT
Ms4a3^FlpO
0%
97.2%
Ly6C (BV421)
TdTomato
j
Ms4a3^FlpO x R26^FSF-tdTomato
BAT
Monocytes
CD206⁻ CD226⁻
CD226^high
CD206^high
% TdTomato⁺
2 months
6 months
k
C57BL/6J
i.p
MC-21 or PBS
Monocytes
CD206⁻ CD226⁻
CD226^high
CD206^high
Cells / mg of BAT (fold changes)
0.0545
MC-21 administration (days)

Figure 1. Characterization of brown adipose tissue CD226^{high} macrophages.
(**a**) Trajectory analysis of BAT myeloid cells using Slingshot. (**b, c**) Analysis of Timd4 (b) and CX3CR1^{GFP} (c) expression in BAT macrophages. (**d**) Fate mapping analysis of monocyte contribution to CX3CR1^{+} and CX3CR1^{-} BAT macrophages in CCR2^{CreERT2}; R26^{tdTomato}; CX3CR1^{GFP} mice that received tamoxifen gavage two days prior. (**e**) Fate mapping analysis of CX3CR1^{+} BAT macrophages using double reporter CX3CR1$^{CreERT2/GFP}$; R26^{tdTomato} mice. (**f**) Time-course analysis of BAT monocyte and macrophage tdTomato labeling following tamoxifen administration in Ms4a3^{CreERT2}; R26^{tdTomato} mice. (**g**) Schematic representation of the macrophage lineage tracing strategy using the double fate-mapping model Tnfrsf11a^{Cre}; Rosa26$^{LSL-YFP}$; Ms4a3^{FlpO}; Rosa26$^{FSF-tdTomato}$. *Tnfrsf11a* is expressed in pre-macrophages (pMac) originating from yolk sac erythro-myeloid progenitors (EMP). Long-lived macrophages derived from the yolk sac are marked by the yellow fluorescent protein (YFP) signal, depicted in green. *Ms4a3* is expressed in granulocyte-monocyte progenitors (GMP), which arise from hematopoietic stem cells (HSC) during definitive hematopoiesis. Short-lived or recently differentiated monocyte-derived macrophages are labeled with tdTomato, represented in red. If a monocyte-derived macrophage persists in the tissue, *Tnfrsf11a* is upregulated, triggering recombination at the Rosa26$^{LSL-YFP}$ locus and resulting in co-expression of both YFP and tdTomato, indicated by a yellow signal. (**h**) Flow cytometry analysis of tdTomato and YFP expression in BAT CD226^{high} and CD206^{high} macrophages from Ms4a3^{Flp}; R26$^{FSF-tdTomato}$; Tnfrsf11a^{Cre}; R26$^{LSL-YFP}$ mice. (**i**) Flow cytometry analysis of tdTomato expression in blood monocytes from Ms4a3^{Flp}; R26$^{FSF-tdTomato}$ mice. (**j**) Quantification of tdTomato^{+} cells among the indicated BAT monocyte and macrophage populations in Ms4a3^{Flp}; R26$^{FSF-tdTomato}$ mice. (**k**) Time-course quantification of BAT macrophage subsets along MC-21 administration. Data are presented as mean values +/- SEM. See also Figures S1 and S2.

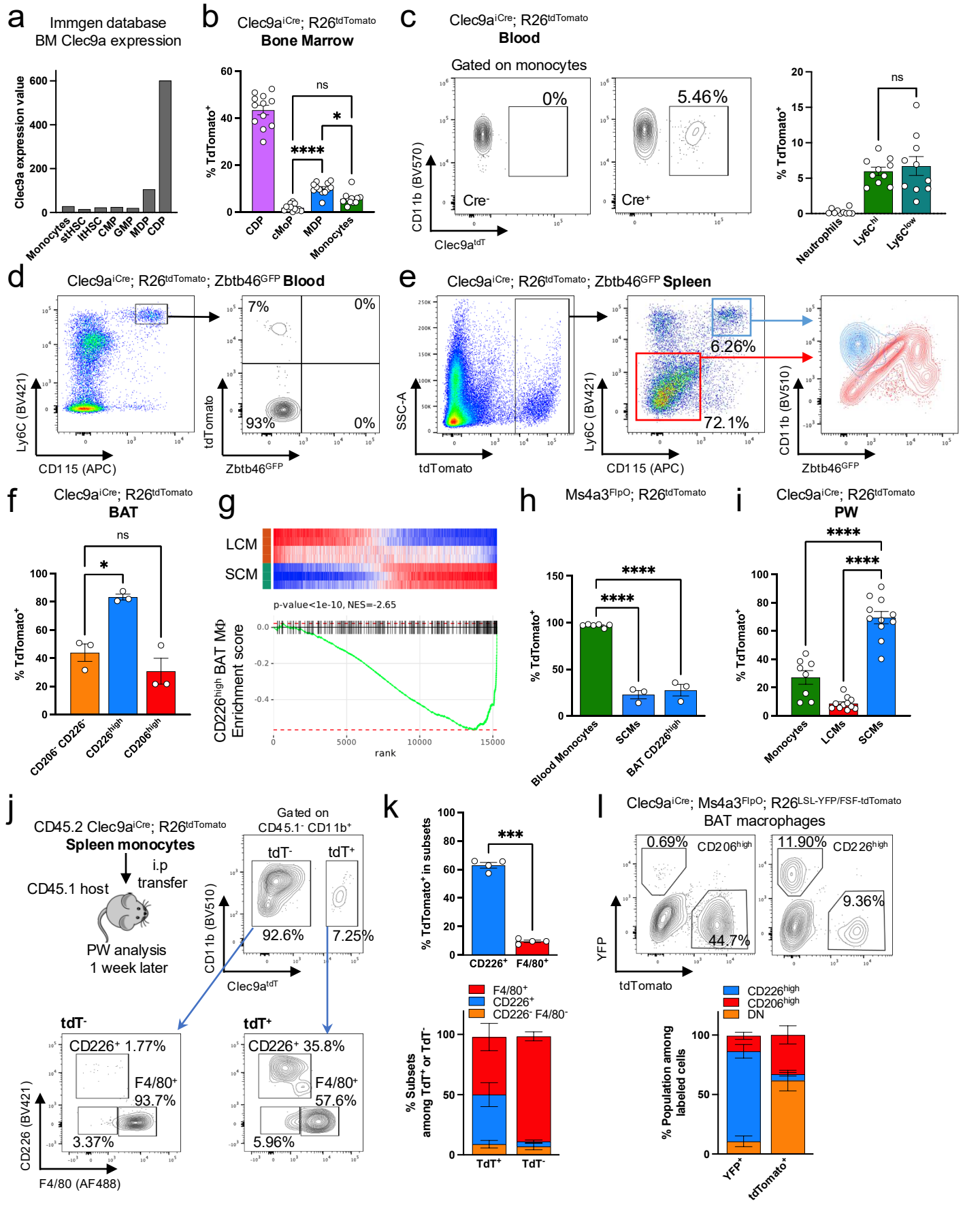
a
Immgen database
BM Clec9a expression
Clec9a expression value
Monocytes
stHSC
itHSC
CMP
GMP
MDP
CDP
b
Clec9a^{iCre}; R26^{tdTomato}
Bone Marrow
% TdTomato$^+$
ns
****
*
CDP
cMoP
MDP
Monocytes
c
Clec9a^{iCre}; R26^{tdTomato}
Blood
Gated on monocytes
0%
5.46%
Cre$^-$
Cre$^+$
CD11b (BV570)
Clec9a^{tdT}
% TdTomato$^+$
ns
Neutrophils
Ly6C^{hi}
Ly6C^{low}
d
Clec9a^{iCre}; R26^{tdTomato}; Zbtb46^{GFP} Blood
Ly6C (BV421)
CD115 (APC)
7%
0%
93%
0%
tdTomato
Zbtb46^{GFP}
e
Clec9a^{iCre}; R26^{tdTomato}; Zbtb46^{GFP} Spleen
SSC-A
tdTomato
6.26%
72.1%
Ly6C (BV421)
CD115 (APC)
CD11b (BV510)
Zbtb46^{GFP}
f
Clec9a^{iCre}; R26^{tdTomato}
BAT
% TdTomato$^+$
ns
*
CD206$^-$ CD226$^-$
CD226^{high}
CD206^{high}
g
LCM
SCM
p-value<1e-10, NES=-2.65
CD226^{high} BAT MΦ Enrichment score
rank
h
Ms4a3^{FlpO}; R26^{tdTomato}
% TdTomato$^+$
****
****
Blood Monocytes
SCMs
BAT CD226^{high}
i
Clec9a^{iCre}; R26^{tdTomato}
PW
% TdTomato$^+$
****
****
Monocytes
LCMs
SCMs
j
CD45.2 Clec9a^{iCre}; R26^{tdTomato}
Spleen monocytes
i.p
transfer
CD45.1 host
PW analysis
1 week later
Gated on
CD45.1$^-$ CD11b$^+$
tdT$^-$
tdT$^+$
92.6%
7.25%
CD11b (BV510)
Clec9a^{tdT}
tdT$^-$
CD226$^+$ 1.77%
F4/80$^+$
93.7%
3.37%
tdT$^+$
CD226$^+$ 35.8%
F4/80$^+$
57.6%
5.96%
CD226 (BV421)
F4/80 (AF488)
k
% TdTomato$^+$ in subsets
***
CD226$^+$
F4/80$^+$
F4/80$^+$
CD226$^+$
CD226$^-$ F4/80$^-$
% Subsets among TdT$^+$ or TdT$^-$
TdT$^+$
TdT$^-$
l
Clec9a^{iCre}; Ms4a3^{FlpO}; R26$^{LSL-YFP/FSF-tdTomato}$
BAT macrophages
0.69%
CD206^{high}
44.7%
11.90%
CD226^{high}
9.36%
YFP
tdTomato
CD226^{high}
CD206^{high}
DN
% Population among labeled cells
YFP$^+$
tdTomato$^+$

Figure 2

Figure 2. CD226^{high} macrophages develop from MDP-derived monocytes.

(**a**) Expression of *Clec9a* mRNA by bone marrow (BM) short term hematopoietic stem cells (stHSC), long term hematopoietic stem cells (ltHSC), common myeloid progenitors (CMP), granulocyte monocyte progenitors (GMP), monocyte dendritic cell progenitors (MDP), common dendritic cell progenitors (CDP) and monocytes. Data from Immgen.org. (**b**) Quantification of tdTomato^{+} cells among bone marrow progenitors and monocytes in Clec9a^{iCre}; R26^{tdTomato} mice. (**c**) Quantification of tdTomato^{+} cells among blood neutrophils and monocytes in Clec9a^{iCre}; R26^{tdTomato} mice. (**d-e**) Flow cytometry analysis of blood (d) and spleen (e) Ly6C^{high} monocytes from Clec9a^{iCre}; R26^{tdTomato}; Zbtb46^{GFP} mice. (**f**) Quantification of tdTomato^{+} cells among BAT macrophages in Clec9a^{iCre}; R26^{tdTomato} mice. (**g**) GSEA analysis, comparing the signature of BAT CD226^{high} macrophages to peritoneal LCMs and SCMs. (**h**) Quantification of tdTomato^{+} cells among blood monocytes, peritoneal SCMs and BAT CD226^{high} macrophages in Ms4a3^{FlpO}; R26^{tdTomato} mice. (**i**) Quantification of tdTomato^{+} cells among peritoneal monocytes and macrophages in Clec9a^{iCre}; R26^{tdT} mice. (**j**) Experimental design and representative flow cytometry plots showing phenotype of tdTomato^{+} and tdTomato^{-} monocytes from Clec9a^{iCre}; R26^{tdT} mice that were adoptively transferred intraperitoneally. (**k**) Quantification of tdTomato^{+} cells among peritoneal wash F4/80^{+} and CD226^{high} cells following adoptive transfer as in (j). (**l**) Representative flow cytometry plots showing YFP and tdTomato expression among BAT macrophages (top) and proportions of macrophage subsets among YFP^{+} or TdTomato^{+} cells (bottom) from Clec9a^{iCre}; Ms4a3^{FlpO}; R26$^{LSL-YFP/FSF-tdTomato}$ mice. Data are presented as mean values +/- SEM. See also Figure S3.

Figure 3

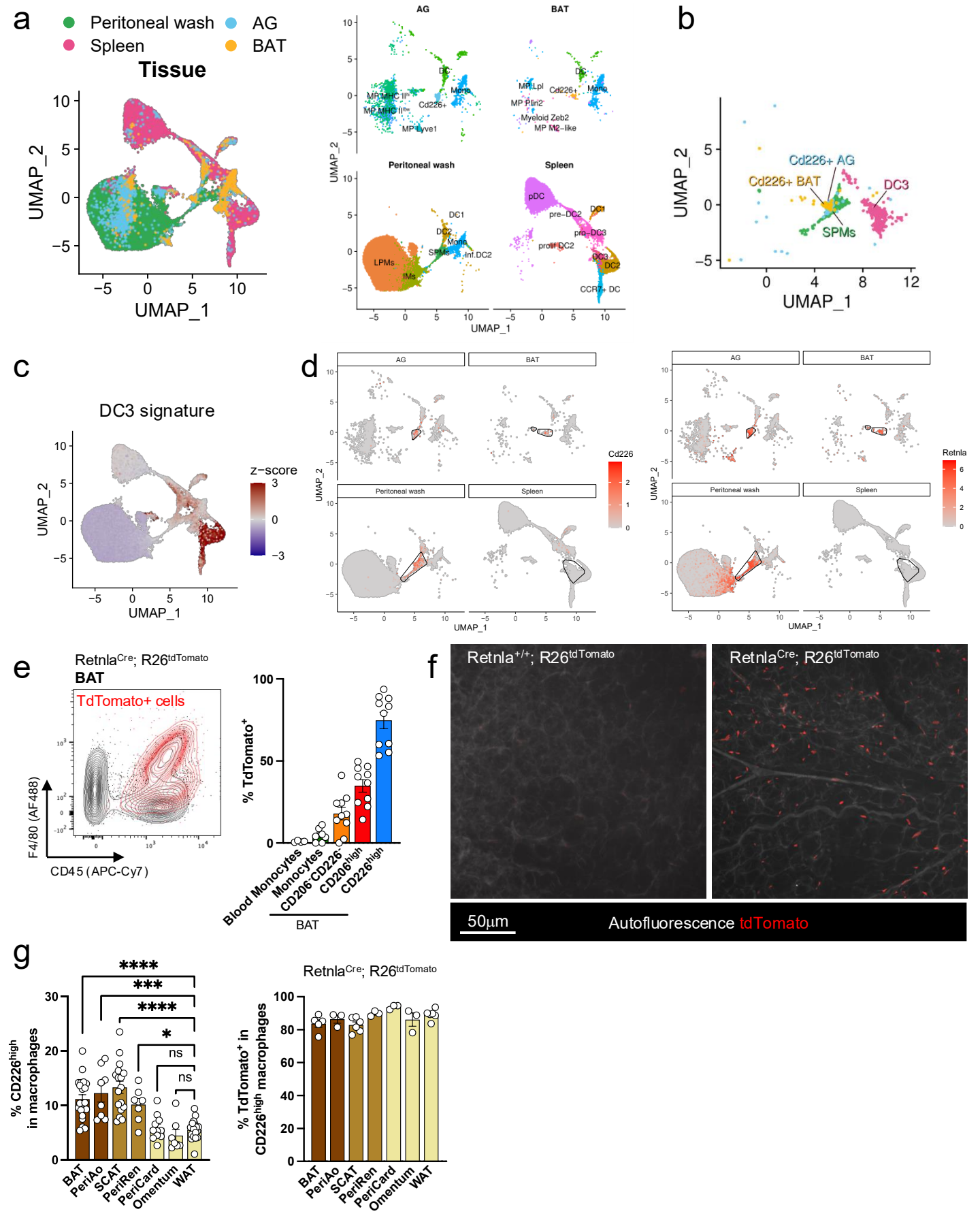

a
Peritoneal wash
AG
Spleen
BAT
Tissue
UMAP_2
UMAP_1
AG
BAT
Peritoneal wash
Spleen
DC
Mono
Cd226+
MP MHC II
MP Lyve1
MP Lpl
MP Plin2
Myeloid Zeb2
MP M2-like
DC1
DC2
SPMs
Inf.DC2
LPMs
IMs
pDC
pre-DC2
pro-DC3
prolif DC2
CCR7+ DC
b
Cd226+ AG
Cd226+ BAT
DC3
SPMs
c
DC3 signature
z-score
d
Cd226
Retnla
e
Retnla^Cre; R26^tdTomato
BAT
TdTomato+ cells
F4/80 (AF488)
CD45 (APC-Cy7)
% TdTomato+
Blood Monocytes
Monocytes
CD206-CD226-
CD206high
CD226high
BAT
f
Retnla+/+; R26tdTomato
Retnla^Cre; R26^tdTomato
50μm
Autofluorescence tdTomato
g
% CD226high in macrophages
****
***
****
*
ns
ns
BAT
PeriAo
SCAT
PeriRen
PeriCard
Omentum
WAT
Retnla^Cre; R26^tdTomato
% TdTomato+ in CD226high macrophages

Figure 3. CD226^{high} macrophages are conserved across tissues and enriched in thermogenic adipose tissue. (**a**) Single cell RNA-sequencing analysis of integrated datasets of immune cells from BAT, adrenal glands (AG) and peritoneal wash, and Flt3^{+} cells from spleen. (**b**) UMAP plot representing clustering of CD226^{high} macrophages from BAT, AGs and peritoneal wash, and DC3 from spleen. (**c**) UMAP plot representing expression of the DC3 signature by all cells contained in the integrated dataset from (a). (**d**) Expression of *Cd226* and *Retnla* by BAT, AG, peritoneal wash and spleen immune cells. (**e**) Flow cytometry plot showing distribution of tdTomato^{+} cells from Retnla^{cre}; R26^{tdTomato} mice in BAT (left) and quantification of tdTomato expression by blood and BAT monocytes and BAT macrophages (right). (**f**) Confocal microscopy analysis of BAT from Retnla$^{+/+}$; R26^{tdTomato} and Retnla$^{Cre/+}$; R26^{tdTomato} mice. (**g**) Quantification of F4/80^{+} CD64^{low} CD226^{high} macrophages (left) and their expression of tdTomato in Retnla^{cre}; R26^{tdTomato} mice (right) in interscapular BAT, peri-aortic brown adipose tissue (PeriAo), subcutaneous adipose tissue (SCAT), peri-renal adipose tissue (PeriRen), peri-cardiac adipose tissue (PeriCard), omentum and gonadal white adipose tissue (WAT). Data are presented as mean values +/- SEM. See also Figure S4.

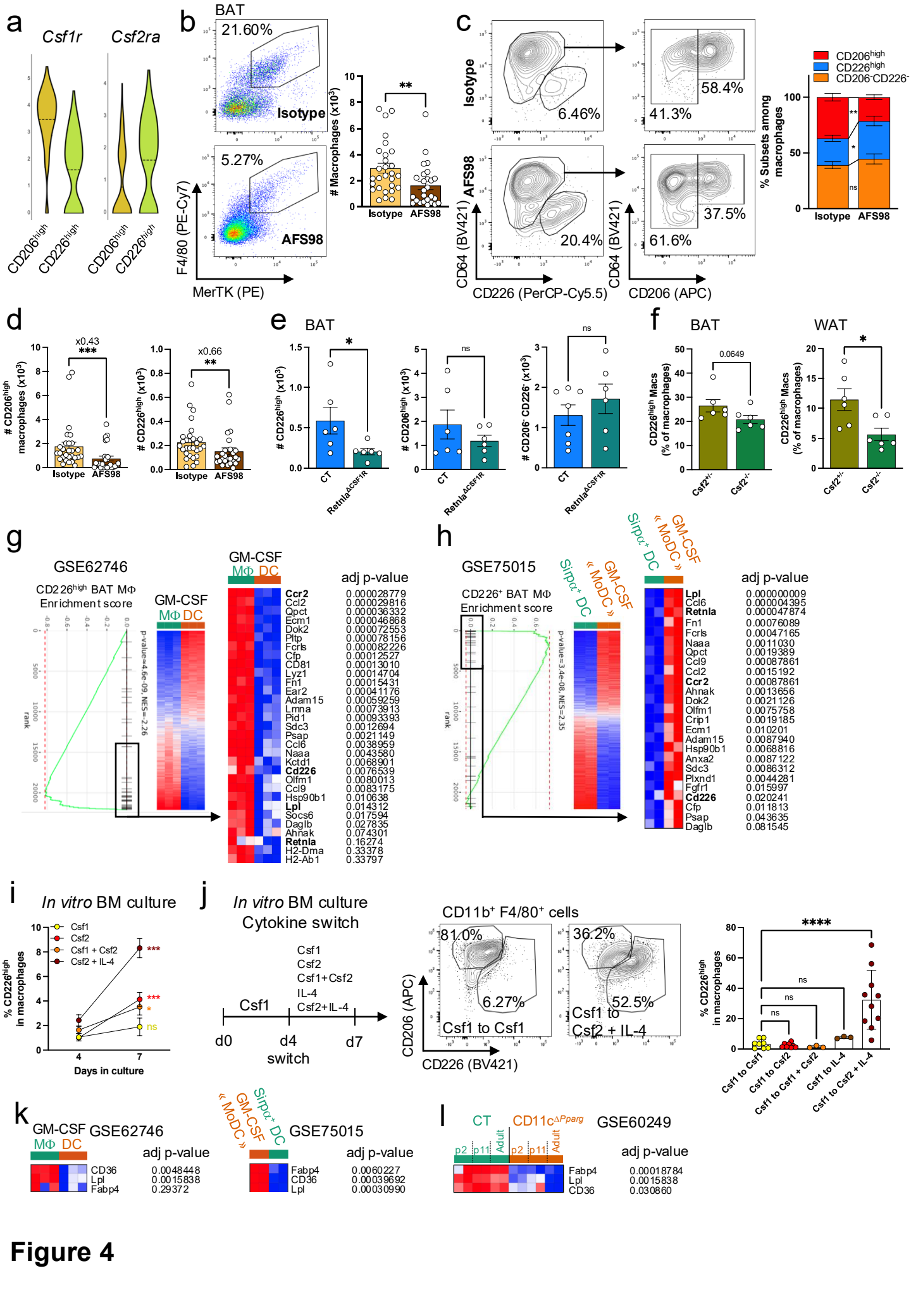
a
Csf1r
Csf2ra
CD206high
CD226high
b
BAT
21.60%
Isotype
5.27%
AFS98
F4/80 (PE-Cy7)
MerTK (PE)
Macrophages (x10³)
Isotype
AFS98
c
Isotype
6.46%
58.4%
41.3%
AFS98
20.4%
37.5%
61.6%
CD64 (BV421)
CD226 (PerCP-Cy5.5)
CD206 (APC)
CD206high
CD226high
CD206-CD226-
% Subsets among macrophages
d
x0.43
x0.66
CD206high macrophages (x10³)
CD226high (x10³)
e
BAT
CD226high (x10³)
CD206high (x10³)
CD206- CD226- (x10³)
CT
RetnlaΔCSF1R
f
BAT
WAT
0.0649
CD226high Macs (% of macrophages)
Csf2+/-
Csf2-/-
g
GSE62746
CD226high BAT MΦ Enrichment score
GM-CSF
MΦ DC
adj p-value
Ccr2 0.000028779
Ccl2 0.000029816
Qpct 0.000036332
Ecm1 0.000046868
Dok2 0.000072553
Pltp 0.000078156
Fcrls 0.000082226
Cfp 0.00012527
CD81 0.00013010
Lyz1 0.00014704
Fn1 0.00015431
Ear2 0.00041176
Adam15 0.00059259
Lmna 0.00073913
Pid1 0.00093393
Sdc3 0.0012694
Psap 0.0021149
Ccl6 0.0038959
Naaa 0.0043580
Kctd1 0.0068901
Cd226 0.0076539
Olfm1 0.0080013
Ccl9 0.0083175
Hsp90b1 0.010638
Lpl 0.014312
Socs6 0.017594
Daglb 0.027835
Ahnak 0.074301
Retnla 0.16274
H2-Dma 0.33378
H2-Ab1 0.33797
h
GSE75015
CD226+ BAT MΦ Enrichment score
Sirpα+ DC
GM-CSF « MoDC »
adj p-value
Lpl 0.000000009
Ccl6 0.000004395
Retnla 0.000047874
Fn1 0.00076089
Fcrls 0.00047165
Naaa 0.0011030
Qpct 0.0019389
Ccl9 0.00087861
Ccl2 0.0015192
Ccr2 0.00087861
Ahnak 0.0013656
Dok2 0.0021126
Olfm1 0.0075758
Crip1 0.0019185
Ecm1 0.010201
Adam15 0.0087940
Hsp90b1 0.0068816
Anxa2 0.0087122
Sdc3 0.0086312
Plxnd1 0.0044281
Fgfr1 0.015997
Cd226 0.020241
Cfp 0.011813
Psap 0.043635
Daglb 0.081545
i
In vitro BM culture
Csf1
Csf2
Csf1 + Csf2
Csf2 + IL-4
% CD226high in macrophages
Days in culture
j
In vitro BM culture
Cytokine switch
Csf1
Csf2
Csf1+Csf2
IL-4
Csf2+IL-4
d0
d4
d7
switch
CD11b+ F4/80+ cells
81.0%
6.27%
Csf1 to Csf1
36.2%
52.5%
Csf1 to Csf2 + IL-4
CD206 (APC)
CD226 (BV421)
% CD226high in macrophages
Csf1 to Csf1
Csf1 to Csf2
Csf1 to Csf1 + Csf2
Csf1 to IL-4
Csf1 to Csf2 + IL-4
k
GM-CSF GSE62746
MΦ DC
adj p-value
CD36 0.0048448
Lpl 0.0015838
Fabp4 0.29372
GSE75015
adj p-value
Fabp4 0.0060227
CD36 0.00039692
Lpl 0.00030990
l
CT
CD11cΔPparg
GSE60249
p2
p11
Adult
adj p-value
Fabp4 0.00018784
Lpl 0.0015838
CD36 0.030860

Figure 4

Figure 4. CSF1R and GM-CSF regulate CD226^{high} macrophages.

(**a**) Violin plots representing *Cs1r* and *Csf2ra* expression by BAT CD226^{high} and CD206^{high} macrophages. (**b-d**) Representative flow cytometry plots and quantifications of total BAT macrophages (b) and BAT macrophage subset numbers (c) and proportions (d) following CD115 blockade using AFS98. (**e**) Quantification of BAT macrophage susbets in control (CT) and Retnla$^{\Delta CSF1R}$ mice. (**f**) Quantification of BAT macrophage subsets in Csf2$^{+/-}$ and Csf2$^{-/-}$ mice. (**g, h**) GSEA analysis and differential gene expression analysis, comparing the signature of BAT CD226^{high} macrophages to macrophages and DCs obtained by culturing bone marrow with GM-CSF (g) or conventional Sirpα^{+} DCs and "MoDCs" obtained with GM-CSF culture (h). (**i**) Flow cytometry analysis of total bone marrow cells cultured with M-CSF (50ng/mL), GM-CSF (50ng/mL) with or without IL-4 (10ng/mL), or M-CSF + GM-CSF (50ng/mL) for 4 or 7 days. (**j**) Flow cytometry analysis of total bone marrow cells cultured with M-CSF for 4 days, and then with M-CSF, GM-CSF with or without IL-4, or M-CSF + GM-CSF for another 3 days.(**k, l**) Expression of *Cd36*, *Fabp4* and *Lpl* measured in GM-CSF derived macrophages and dendritic cells (k) or alveolar macrophages from new born (p2, p11) or adult (7-8 weeks) control (CT) and CD11^{cre}; Pparg$^{fl/fl}$ mice (l). Data are presented as mean values +/- SEM. See also Figure S5.

Figure 5

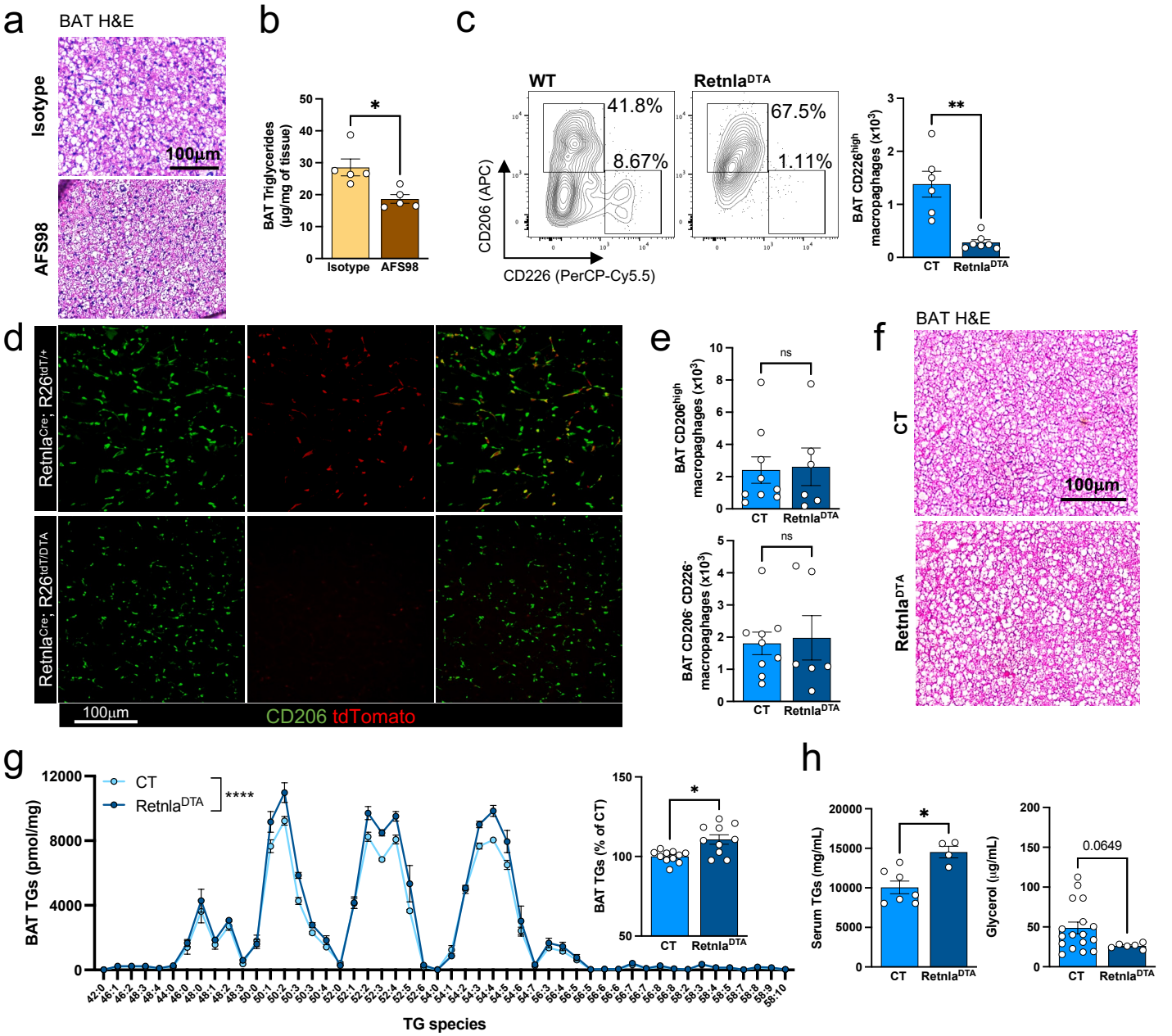

Figure 5. CD226^{high} macrophages regulate triglyceride metabolism.
(**a-b**) Hematoxylin and eosin staining of BAT (a) and quantification of BAT triglyceride content (b) following AFS98 treatment. (**c**) Representative flow cytometry plots (left) and quantification (right) of BAT CD226^{high} macrophages in control (CT) and Retnla^{Cre}; R26^{DTA} mice. (**d**) Confocal microscopy analysis of BAT from Retnla^{Cre}; R26$^{tdT/DTA}$ and control Retnla^{Cre}; R26$^{tdT/+}$ mice. (**e**) Representative flow cytometry plots (left) and quantification (right) of BAT CD206^{high} and CD206^{-} CD226^{-} macrophages in control and Retnla^{Cre}; R26^{DTA} mice. (**f, g**) Hematoxylin and eosin staining of BAT (e) and triglyceride content analyzed using lipidomics (f) in Retnla^{Cre}; R26^{DTA} mice. (**g**) Quantification serum triglyceride (TG) and glycerol levels in Retnla^{Cre}; R26^{DTA} mice. Data are presented as mean values +/- SEM. See also Figure S6.